

Nonresonant Raman and inelastic X-ray scattering in the charge-density-wave phase of the spinless Falicov-Kimball model

O. P. Matveev,¹ A. M. Shvaika,¹ and J. K. Freericks²

¹*Institute for Condensed Matter Physics of the National Academy of Sciences of Ukraine, Lviv, 79011 Ukraine*

²*Department of Physics, Georgetown University, Washington, DC 20057, U.S.A.*

Nonresonant inelastic light and X-ray scattering is investigated for the spinless Falicov-Kimball model on an infinite-dimensional hypercubic lattice with a charge-density-wave phase at half filling. The many-body density of states (DOS) is found for different values of the Coulomb repulsion U , ranging from a dirty metal to a Mott insulator. At zero temperature, the charge gap is exactly equal to U ; increasing the temperature rapidly fills the gap with subgap states. The nonresonant response function for Raman and inelastic X-ray scattering shows peaks connected with transitions over the gap and transitions that involve subgap states. In the case of X-ray scattering (when both energy and momentum are transferred), the response function illustrates features of dynamical screening (vertex corrections) in the different (nonresonant) symmetry channels (A_{1g} and B_{1g}). We also derive and verify the first moment sum rules for the (nonresonant) Raman and inelastic X-ray response functions.

PACS numbers: 71.10.Fd, 71.45.Lr, 78.30.-j

I. INTRODUCTION

Charge-density wave (CDW) systems possess a static rearrangement of the charge that is modulated by their ordering vector. Since the underlying ionic cores are charged, they will respond to this charge modulation from the electrons, and often create a distorted lattice structure that follows the modulated charge order of the electrons. This is often one of the easiest to measure signals of CDW order, namely the distortion of the unit cell due to the ionic displacement that goes hand-in-hand with the electronic charge modulation.

In this work, we focus on signatures of the CDW order that are present in inelastic light scattering experiments on CDW systems. Since inelastic Raman scattering is sensitive to different symmetry charge modulations (when polarizers are used on the incident and scattered light), they can provide information about the symmetry of the CDW state. Similarly, because inelastic X-ray scattering also allows for an exchange of momentum by the scattered photon, we might anticipate interesting behavior to occur when the ordering wavevector and the transferred momentum are the same.

We develop all of the formalism to generalize the dynamical mean-field theory (DMFT) approach to inelastic Raman and X-ray scattering to include the situation when there is a CDW phase on a bipartite lattice with an ordering wavevector equal to (π, π, \dots, π) ; our formulas include all effects of vertex corrections including dynamical screening. While the formal development, in terms of Green's functions, self-energies, and irreducible vertex functions, is completely general, we analyze the formalism for the specific case of the Falicov-Kimball model because the irreducible charge vertex is known, and we can determine all of our results exactly. In addition to deriving formulas for the light scattering spectra, we also examine the first moment sum rules for these spectra, which are equal to expectation values related to the ki-

netic and potential energies of the material.

We anticipate our results should be relevant to different experimental systems that display charge-density-wave order on a bipartite lattice, especially in compounds which are three-dimensional like¹ BaBiO_3 and $\text{Ba}_{1-x}\text{K}_x\text{BiO}_3$, because DMFT is most accurate in higher dimensional systems. Our work also extends recent results on transport and optical conductivity in CDW systems^{2,3} to the realm of inelastic light scattering.

The manuscript is organized as follows: In Sec. II, we derive the formalism for inelastic light scattering in a symmetry broken phase including explicit expressions for Raman scattering, inelastic X-ray scattering, and their first moment sum rules. In Sec. III, we present our numerical results and discuss what signatures are likely to be seen in experiment. Our conclusions are presented in Sec. IV.

II. FORMALISM

Since CDW ordering is a static order, it is often well described by static models like the Falicov-Kimball model⁴. This model was introduced in 1969 to describe metal-insulator transitions in rare-earth compounds and transition-metal oxides. Since then, it has been studied widely within the DMFT community, primarily because it is one of the simplest many-body problems that admits an exact solution⁵ (for a review see Ref. 6). The Falicov-Kimball model has two kinds of particles: mobile electrons and localized electrons. Mobile electrons hop from site to site with a hopping integral between nearest neighbors and they interact with the localized electrons when both sit on the same site (the interaction energy is U); we denote the mobile electron creation (annihilation) operator at site i by \hat{d}_i^\dagger (\hat{d}_i) and the local electron creation (annihilation) operator at site i by \hat{f}_i^\dagger (\hat{f}_i).

The model has commensurate CDW order at half filling and this is the main property we exploit here. Brandt and Mielsch worked out the formalism for calculating the ordered-phase Green's functions⁷ shortly after Metzner and Vollhardt introduced the idea of the many-body problem simplifying in large dimensions⁸. The CDW order parameter was shown to display anomalous behavior at weak coupling^{9,10}, and higher-period ordered phases have been examined on the Bethe lattice¹¹. Transport calculations in the commensurate CDW phase have also appeared recently^{2,3}.

A. DMFT for the CDW ordered phase

The hypercubic lattice is a bipartite lattice, implying that it separates into two sublattices (called A and B) with the hopping being nonzero only between the two sublattices. In this case, the model will display commensurate (chessboard) CDW order when both the light and heavy particles are half-filled. This CDW order corresponds to the situation where the average filling of the electrons remains uniform on each sublattice, but changes from one sublattice to another (it is commensurate because the lattice is bipartite here). We begin by writing the Falicov-Kimball model Hamiltonian as the sum of its local and nonlocal parts

$$\hat{\mathcal{H}} = \sum_{ia} \hat{\mathcal{H}}_i^a - \sum_{ijab} t_{ij}^{ab} \hat{d}_{ia}^\dagger \hat{d}_{jb}, \quad (1)$$

where i and $a = A$ or B are the site and sublattice indexes, respectively, and t_{ij}^{ab} is the hopping matrix, which is nonzero only between different sublattices ($t_{ij}^{AA} = t_{ij}^{BB} = 0$). The local Hamiltonian is equal to

$$\hat{\mathcal{H}}_i^a = U \hat{n}_{id}^a \hat{n}_{if}^a - \mu_d^a \hat{n}_{id}^a - \mu_f^a \hat{n}_{if}^a; \quad (2)$$

with the number operators of the mobile and localized electrons given by $\hat{n}_{id} = \hat{d}_i^\dagger \hat{d}_i$ and $\hat{n}_{if} = \hat{f}_i^\dagger \hat{f}_i$, respectively. Note that we have introduced different chemical potentials for different sublattices. This is convenient for computations, because it allows us to work with a fixed order parameter, rather than iterating the DMFT equations to determine the order parameter (which is subject to critical slowing down near T_c). Of course, the equilibrium solution occurs when the chemical potential is uniform throughout the system ($\mu_d^A = \mu_d^B$ and $\mu_f^A = \mu_f^B$).

We start with the definition of the lattice Green's function

$$G_{ij}^{ab}(\tau) = -\text{Tr} \left[\mathcal{T}_\tau e^{-\beta \hat{\mathcal{H}}} \hat{d}_{ia}(\tau) \hat{d}_{jb}^\dagger(0) \right] / \mathcal{Z}, \quad (3)$$

$$\mathcal{Z} = \text{Tr} \exp[-\beta \hat{\mathcal{H}}].$$

Within a Feynman-diagram formalism, the Green's function satisfies Dyson's equation (which in fact is a compact form of the diagrammatic series)

$$\sum_{lc} [(\omega + \mu_d^a) \delta_{ac} \delta_{il} - \Sigma_{il}^{ac}(\omega) + t_{il}^{ac}] G_{lj}^{cb}(\omega) = \delta_{ij} \delta_{ab}, \quad (4)$$

where ω is a real frequency. The unperturbed band structure for the hypercubic lattice with nearest neighbor (NN) hopping satisfies

$$\epsilon_{\mathbf{k}} = - \sum_{i-j} t_{ij}^{AB} \exp[i\mathbf{k} \cdot (\mathbf{R}_{iA} - \mathbf{R}_{jB})] = -2t \sum_{\alpha=1}^D \cos k_{\alpha a}, \quad (5)$$

where \mathbf{R}_{iA} is a lattice vector for site i on sublattice A and a is the lattice spacing (we set $a = 1$).

The first step of DMFT is to scale⁸ the hopping matrix element as $t = t^*/2\sqrt{D}$ (we use $t^* = 1$ as the unit of energy) and then take the limit of the infinite dimensions $D \rightarrow \infty$. The self-energy is then local:

$$\Sigma_{ij}^{ab}(\omega) = \Sigma_i^a(\omega) \delta_{ij} \delta_{ab}, \quad (6)$$

and in the case of two sublattices has two values $\Sigma^A(\omega)$ and $\Sigma^B(\omega)$. Now, we can write the solution of the Dyson equation (in a momentum representation) in a matrix form

$$G_{\mathbf{k}}(\omega) = [z(\omega) - t_{\mathbf{k}}]^{-1}, \quad (7)$$

where $z(\omega)$ and the hopping term $t_{\mathbf{k}}$ are represented by the following 2×2 matrices:

$$z(\omega) = \begin{pmatrix} \omega + \mu_d^A - \Sigma^A(\omega) & 0 \\ 0 & \omega + \mu_d^B - \Sigma^B(\omega) \end{pmatrix}, \quad (8)$$

$$t_{\mathbf{k}} = \begin{pmatrix} 0 & \epsilon_{\mathbf{k}} \\ \epsilon_{\mathbf{k}} & 0 \end{pmatrix}.$$

After substituting Eq. (8) into Eq. (7), we obtain three equations for the different Green's function components

$$G_{\mathbf{k}}^{AA}(\omega) = \frac{\omega + \mu_d^B - \Sigma^B(\omega)}{\bar{Z}^2(\omega) - \epsilon_{\mathbf{k}}^2}, \quad (9)$$

$$G_{\mathbf{k}}^{BB}(\omega) = \frac{\omega + \mu_d^A - \Sigma^A(\omega)}{\bar{Z}^2(\omega) - \epsilon_{\mathbf{k}}^2}, \quad (10)$$

$$G_{\mathbf{k}}^{AB}(\omega) = G_{\mathbf{k}}^{BA}(\omega) = \frac{\epsilon_{\mathbf{k}}}{\bar{Z}^2(\omega) - \epsilon_{\mathbf{k}}^2} \quad (11)$$

with $\bar{Z}(\omega)$ defined by

$$\bar{Z}(\omega) = \sqrt{[\omega + \mu_d^A - \Sigma^A(\omega)][\omega + \mu_d^B - \Sigma^B(\omega)]}. \quad (12)$$

These expressions agree with those of Brandt and Mielsch⁷ even though our notation is somewhat different from theirs.

The local Green's functions are now found to be

$$G^{aa}(\omega) = \frac{1}{N} \sum_{\mathbf{k}} G_{\mathbf{k}}^{aa}(\omega) = \frac{\omega + \mu_d^b - \Sigma^b(\omega)}{\bar{Z}(\omega)} F_{\infty}[\bar{Z}(\omega)], \quad (13)$$

where

$$F_{\infty}[\bar{Z}(\omega)] = \int d\epsilon \rho(\epsilon) \frac{1}{\bar{Z}(\omega) - \epsilon} \quad (14)$$

is the Hilbert transform of the noninteracting density of states, which satisfies $\rho(\epsilon) = \exp(-\epsilon^2/t^{*2})/t^* \sqrt{\pi}$ for the infinite-dimensional hypercubic lattice.

The second step of DMFT is to map the lattice Green's function onto a local problem by means of the dynamical mean field. Since there are two sublattices, a dynamical mean field $\lambda^a(\omega)$ is introduced on each of them. As a result, the local lattice Green's function on each sublattice becomes:

$$G^{aa}(\omega) = \frac{1}{\omega + \mu_d^a - \Sigma^a(\omega) - \lambda^a(\omega)}. \quad (15)$$

The third equation that closes the system of equations for $G^{aa}(\omega)$, $\Sigma^a(\omega)$ and $\lambda^a(\omega)$ is obtained from the condition that the local Green's function can be defined as the Green's function of an impurity with the same dynamical mean field $\lambda^a(\omega)$. Such a problem can be exactly solved and the result is equal to

$$G^{aa}(\omega) = \frac{1 - n_f^a}{\omega + \mu_d^a - \lambda^a(\omega)} + \frac{n_f^a}{\omega + \mu_d^a - U - \lambda^a(\omega)}. \quad (16)$$

These equations are self-consistently solved numerically. The iterative DMFT algorithm to calculate the lattice Green's function is as follows: for a fixed value of the order parameter $\Delta n_f = n_f^A - n_f^B$ one chooses n_f^A and n_f^B in such a way that $n_f^A + n_f^B = n_f$ ($n_f = 1/2$ for half filling). With those fixed quantities, we now propose a guess for the self-energy on each sublattice, and then compute the local Green's function from Eqs. (12) and (13). Then we extract the dynamical mean field on each sublattice from Eq. (15), and find the local Green's function for the impurity from Eq. (16). This value is substituted into Eq. (15) to calculate the new self-energy. This procedure is repeated until the Green's function converges. In order to find the correct equilibrium order parameter Δn_f at the given temperature, one calculates the chemical potentials for the f -electrons on each sublattice via

$$\begin{aligned} \mu_f^a &= -\frac{U}{2} - T \ln \frac{1 - n_f^a}{n_f^a} \\ &- T \sum_n \ln \left[1 - \frac{U}{i\omega_n + \mu_d^a - \lambda^a(i\omega_n)} \right], \end{aligned} \quad (17)$$

where we introduce the fermionic Matsubara frequencies $i\omega_n = i\pi T(2n + 1)$. Then Δn_f is extracted from the equilibrium condition $\mu_d^A - \mu_d^B = 0$. Finally, we repeat this iterative solution on the real axis, with the chemical potentials and fillings fixed at their now known values.

In Ref. 3, we already analyzed the evolution of the DOS in the CDW-ordered phase. We reiterate the main points which will be needed here. At $T = 0$, a real gap develops of magnitude U with square root singularities at the band edges. As the temperature increases, the system develops substantial subgap DOS which are thermally activated within the ordered phase. Plots of the DOS can be found in Ref. 3. Note that the singular behavior occurs for one

of the ‘‘inner’’ band edges on each sublattice, and that the subgap states develop very rapidly as the temperature rises.

B. Nonresonant inelastic scattering

Now we develop the formalism for nonresonant light scattering in the CDW phase. We start from the standard formula for the inelastic light scattering cross section derived by Shastry and Shraiman¹²

$$\begin{aligned} R(\mathbf{q}, \Omega) &= 2\pi \sum_{i,f} \frac{e^{-\beta\epsilon_i}}{\mathcal{Z}} \delta(\epsilon_f - \epsilon_i - \Omega) \\ &\times \left| g(\mathbf{k}_i) g(\mathbf{k}_f) e_\alpha^i e_\beta^f \langle f | \hat{M}^{\alpha\beta}(\mathbf{q}) | i \rangle \right|^2. \end{aligned} \quad (18)$$

It describes the scattering of band electrons by photons with $\Omega = \omega_i - \omega_f$ and $\mathbf{q} = \mathbf{k}_i - \mathbf{k}_f$ being the transferred energy and momentum, respectively, $e^{i(f)}$ is the polarization of the initial (final) states of the photons and $\epsilon_{i(f)}$ denotes the electronic eigenstates. The quantity $g(\mathbf{q}) = (\hbar c^2/V\omega_{\mathbf{q}})^{1/2}$ is called the ‘‘scattering strength’’ with $\omega_{\mathbf{q}} = c|\mathbf{q}|$. The scattering operator $\hat{M}(\mathbf{q})$ is constructed from both the number current operator and the stress tensor which are equal to

$$j_\alpha(\mathbf{q}) = \sum_{abk} \frac{\partial t_{ab}(\mathbf{k})}{\partial k_\alpha} \hat{d}_a^\dagger(\mathbf{k} + \mathbf{q}/2) \hat{d}_b(\mathbf{k} - \mathbf{q}/2) \quad (19)$$

and

$$\gamma_{\alpha,\beta}(\mathbf{q}) = \sum_{abk} \frac{\partial^2 t_{ab}(\mathbf{k})}{\partial k_\alpha \partial k_\beta} \hat{d}_a^\dagger(\mathbf{k} + \mathbf{q}/2) \hat{d}_b(\mathbf{k} - \mathbf{q}/2), \quad (20)$$

respectively. Here $t_{ab}(\mathbf{k})$ are the components of the 2×2 hopping matrix in Eq. (8). The interaction of an electronic system with a weak external transverse electromagnetic field \mathbf{A} is described by the Hamiltonian

$$\begin{aligned} H_{\text{int}} &= -\frac{e}{\hbar c} \sum_{\mathbf{k}} \mathbf{j}(\mathbf{k}) \cdot \mathbf{A}(-\mathbf{k}) \\ &+ \frac{e^2}{2\hbar^2 c^2} \sum_{\mathbf{k}\mathbf{k}'} A_\alpha(-\mathbf{k}) \gamma_{\alpha,\beta}(\mathbf{k} + \mathbf{k}') A_\beta(-\mathbf{k}'). \end{aligned} \quad (21)$$

The scattering operator M is then constructed from these interaction terms; it has both nonresonant and resonant contributions

$$\begin{aligned} \langle f | \hat{M}^{\alpha\beta}(\mathbf{q}) | i \rangle &= \langle f | \gamma_{\alpha,\beta}(\mathbf{q}) | i \rangle \\ &+ \sum_l \left(\frac{\langle f | j_\beta(\mathbf{k}_f) | l \rangle \langle l | j_\alpha(-\mathbf{k}_i) | i \rangle}{\epsilon_l - \epsilon_i - \omega_i} \right. \\ &\left. + \frac{\langle f | j_\alpha(-\mathbf{k}_i) | l \rangle \langle l | j_\beta(\mathbf{k}_f) | i \rangle}{\epsilon_l - \epsilon_i + \omega_f} \right) \end{aligned} \quad (22)$$

with the sum l over intermediate states, and after substituting into the cross section formula, one obtains three terms: a pure resonant term; a nonresonant term; and a mixed term (because it is constructed from the square of the scattering operator).

The nonresonant contribution is

$$R_N(\mathbf{q}, \Omega) = 2\pi g^2(\mathbf{k}_i) g^2(\mathbf{k}_f) \quad (23)$$

$$\times \sum_{i,f} \frac{\exp(-\beta\varepsilon_i)}{\mathcal{Z}} \tilde{\gamma}_{i,f} \tilde{\gamma}_{f,i} \delta(\varepsilon_f - \varepsilon_i - \Omega).$$

The tilde denotes contractions with the polarization vectors:

$$\tilde{\gamma} = \sum_{\alpha\beta} e^i_{\alpha} \gamma_{\alpha,\beta}(\mathbf{q}) e^f_{\beta} \quad (24)$$

with the notation $\mathcal{O}_{i,f} = \langle i | \mathcal{O} | f \rangle$ for the matrix elements of an operator \mathcal{O} . (Resonant and mixed diagrams will be examined elsewhere.)

The next step is to evaluate the summations in Eq. (23) via Green's function techniques. In general, such a procedure is nontrivial. But for the nonresonant contribution it is relatively straightforward^{13,14}. We start from the Matsubara function built on two time dependent stress-tensor operators

$$\chi_{\tilde{\gamma},\tilde{\gamma}}(\tau - \tau') = \text{Tr} \left[\mathcal{T}_{\tau} e^{-\beta\hat{H}} \tilde{\gamma}(\tau) \tilde{\gamma}(\tau') \right] / \mathcal{Z}. \quad (25)$$

The imaginary time dependence of the stress-tensor operator is evolved (in the Heisenberg representation) with respect to the equilibrium Hamiltonian because this is a linear-response calculation. The symbol \mathcal{T}_{τ} is a time ordering operator. Further, we perform a Fourier transformation to the imaginary Matsubara frequencies. In thermal equilibrium, the two-particle correlation function depends only on the difference of the two time variables and our Matsubara frequency dependent function can be evaluated as

$$\chi_{\tilde{\gamma},\tilde{\gamma}}(i\nu) = \sum_{i,f} \frac{\exp(-\beta\varepsilon_i)}{\mathcal{Z}} \frac{\tilde{\gamma}_{i,f} \tilde{\gamma}_{f,i}}{\varepsilon_f - \varepsilon_i - i\nu} \quad (26)$$

$$\times [1 - \exp(\beta(\varepsilon_i - \varepsilon_f))].$$

Performing an analytic continuation to the real axis $i\nu \rightarrow \Omega \pm i0^+$ produces the known expression

$$R_N(\mathbf{q}, \Omega) = \frac{2\pi g^2(\mathbf{k}_i) g^2(\mathbf{k}_f)}{1 - \exp(-\beta\Omega)} \chi_N(\mathbf{q}, \Omega), \quad (27)$$

where we introduced the nonresonant response function

$$\chi_N(\mathbf{q}, \Omega) = \frac{1}{\pi} \text{Im} \chi_{\tilde{\gamma},\tilde{\gamma}}(\Omega + i0^+). \quad (28)$$

Now we have reduced the problem to that of finding the response function built on two stress-tensor operators. Actually, such a function corresponds to a two-particle Green's function that will be shortly presented

in Feynman diagrammatic notation. The Fourier transform of the two stress-tensor correlation function can be represented as a sum over Matsubara frequencies of the “generalized polarizations”

$$\chi_{\tilde{\gamma},\tilde{\gamma}}(i\nu_l) = T \sum_m \Pi_{m,m+l}, \quad (29)$$

where we introduced the shorthand notation $\Pi_{m,m+l} = \Pi(i\omega_m, i\omega_m + i\nu_l)$ for the dependence on the fermionic $i\omega_m = i\pi T(2m + 1)$ and bosonic $i\nu_l = i2\pi Tl$ Matsubara frequencies. In the case of the CDW ordered phase, the Feynman diagrams for the “generalized polarizations” $\Pi_{m,m+l}$ are shown in Fig. 1, where we introduce additional sublattice indexes a to l . Here, we used the fact

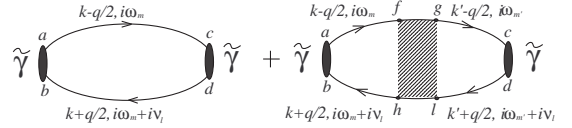


FIG. 1: The Feynman diagrams for the generalized polarizations. Due to the properties of the irreducible charge vertex of the Falicov-Kimball model, we will have $m = m'$.

that the total reducible charge vertex (shaded rectangle in Fig. 1) is a diagonal function of frequencies for the Falicov-Kimball model [see Eq. (42) below]. Now one can perform an analytic continuation to the real axis and replace the sum over Matsubara frequencies by an integral over the real axis:

$$\chi_{\tilde{\gamma},\tilde{\gamma}}(i\nu_l) = \frac{1}{2\pi i} \int_{-i\infty}^{+\infty} d\omega f(\omega) \quad (30)$$

$$\times \left[\Pi(\omega - i0^+, \omega + i\nu_l) - \Pi(\omega + i0^+, \omega + i\nu_l) \right.$$

$$\left. + \Pi(\omega - i\nu_l, \omega - i0^+) - \Pi(\omega + i\nu_l, \omega + i0^+) \right],$$

where $f(\omega) = 1 / [\exp(\beta\omega) + 1]$ is the Fermi distribution function. Then the nonresonant response function is expressed directly in terms of the generalized polarizations

$$\chi_N(\mathbf{q}, \Omega) = \frac{2}{(2\pi i)^2} \int_{-\infty}^{+\infty} d\omega [f(\omega) - f(\omega + \Omega)] \quad (31)$$

$$\times \text{Re} \left\{ \Pi(\omega - i0^+, \omega + \Omega + i0^+) \right.$$

$$\left. - \Pi(\omega - i0^+, \omega + \Omega - i0^+) \right\}.$$

The next step is to calculate these generalized polarizations. We consider both cases of inelastic light (Raman) and inelastic X-ray scattering. For Raman scattering, we can approximate $\mathbf{q} = 0$ because the optical photon wavelength is so large, whereas for inelastic X-ray scattering, the transferred momentum is nonzero $\mathbf{q} \neq 0$.

C. Raman scattering: $q = 0$

The non-resonant Raman response function presented in terms of the generalized polarizations in Eq. (31) is reduced to the calculation of the Feynman diagrams in Fig. 1. As a result, our aim is to calculate the sum of the products of the one-particle Green functions calculated in DMFT and the charge vertices. Here, the momentum \mathbf{k} enters not only through the band energy term $\epsilon_{\mathbf{k}}$ [see Eqs. (9-11)] but also through the stress-tensor factors, namely the derivatives $\partial^2 \epsilon(\mathbf{k}) / \partial k_\alpha \partial k_\beta$. Furthermore, the stress-tensor operator is contracted with polarization vectors $\mathbf{e}^{i,f}$, see Eq. (24), which vary for the different symmetries.

There are three symmetries often examined in experimental systems with cubic symmetry. The A_{1g} symmetry has the full symmetry of the lattice and for the hypercubic lattice the incident and scattered light are both polarized along the same diagonal direction, so in large dimensions we take the initial and final polarizations to be $\mathbf{e}^i = \mathbf{e}^f = (1, 1, 1, \dots)$. The stress-tensor amplitude in the case of A_{1g} symmetry (for NN hopping) is equal to minus the band energy

$$\begin{aligned} \bar{\gamma}_{A_{1g}}(\mathbf{k}) &= \sum_{\alpha\beta} e_\alpha^i e_\beta^f \frac{\partial^2 \epsilon(\mathbf{k})}{\partial k_\alpha \partial k_\beta} \\ &= \frac{t^*}{\sqrt{D}} \sum_{\alpha=1}^D \cos k_\alpha = -\epsilon(\mathbf{k}) \end{aligned} \quad (32)$$

The B_{1g} symmetry is a d -wave-like symmetry that involves crossed polarizers along the diagonals. In this case, we take $\mathbf{e}^i = (1, 1, 1, \dots)$ and $\mathbf{e}^f = (-1, 1, -1, \dots)$, so the stress-tensor amplitude is as follows

$$\begin{aligned} \bar{\gamma}_{B_{1g}}(\mathbf{k}) &= \sum_{\alpha\beta} e_\alpha^i e_\beta^f \frac{\partial^2 \epsilon(\mathbf{k})}{\partial k_\alpha \partial k_\beta} \\ &= -\frac{t^*}{\sqrt{D}} \sum_{\alpha=1}^D (-1)^\alpha \cos k_\alpha \end{aligned} \quad (33)$$

Finally, the B_{2g} symmetry is another d -wave-like symmetry rotated by 45 degrees; it requires the polarization vectors to satisfy $\mathbf{e}^i = (1, 0, 1, 0, \dots)$ and $\mathbf{e}^f = (0, 1, 0, 1, \dots)$, and for NN hopping there are no contributions to the nonresonant response in this channel.

We start with the analysis of the B_{1g} symmetry, which is simplest case to examine. Here, the response function is determined only by the first term (bare loop) of the Feynman diagrams in Fig. 1 and there are no contributions from the second one^{13,15} because the stress-tensor factor has momentum dependence that integrates to zero when multiplied by the local charge vertex and summed over all momentum. The expanded form of the diagrams for the generalized polarization in the B_{1g} channel for the CDW chessboard phase is presented in Fig. 2 and is

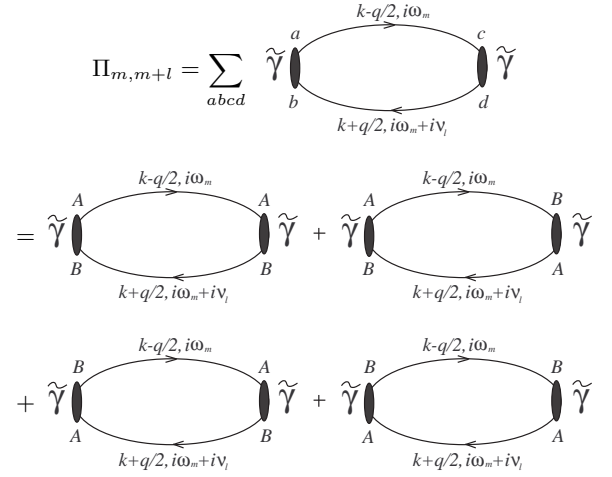


FIG. 2: Individual terms for the bare polarization in the ordered phase.

equal to

$$\begin{aligned} \Pi_{m,m+l} &= \frac{1}{N} \sum_{\mathbf{k}} \bar{\gamma}_{\mathbf{k}}^2 \left(G_{\mathbf{k}-\frac{\mathbf{q}}{2},m}^{AA} G_{\mathbf{k}+\frac{\mathbf{q}}{2},m+l}^{BB} + G_{\mathbf{k}-\frac{\mathbf{q}}{2},m}^{AB} G_{\mathbf{k}+\frac{\mathbf{q}}{2},m+l}^{AB} \right. \\ &\quad \left. + G_{\mathbf{k}-\frac{\mathbf{q}}{2},m}^{BA} G_{\mathbf{k}+\frac{\mathbf{q}}{2},m+l}^{BA} + G_{\mathbf{k}-\frac{\mathbf{q}}{2},m}^{BB} G_{\mathbf{k}+\frac{\mathbf{q}}{2},m+l}^{AA} \right). \end{aligned} \quad (34)$$

After substituting in the expressions for the Green's function in Eqs. (9), (10), and (11), and the expressions for the $\bar{\gamma}_{\mathbf{k}}$ amplitude from Eq. (33), the individual contributions to $\Pi_{m,m+l}$ at $\mathbf{q} = 0$ become

$$\begin{aligned} \frac{1}{N} \sum_{\mathbf{k}} \bar{\gamma}_{\mathbf{k}}^2 G_{\mathbf{k},m}^{AA} G_{\mathbf{k},m+l}^{BB} &= \frac{1}{2} (i\omega_m + \mu_d^B - \Sigma_m^B) \\ &\times (i\omega_m + i\nu_l + \mu_d^A - \Sigma_{m+l}^A) \frac{\frac{F_\infty(\bar{Z}_{m+l})}{\bar{Z}_{m+l}} - \frac{F_\infty(\bar{Z}_m)}{\bar{Z}_m}}{\bar{Z}_m^2 - \bar{Z}_{m+l}^2}, \end{aligned} \quad (35)$$

$$\begin{aligned} \frac{1}{N} \sum_{\mathbf{k}} \bar{\gamma}_{\mathbf{k}}^2 G_{\mathbf{k},m}^{BB} G_{\mathbf{k},m+l}^{AA} &= \frac{1}{2} (i\omega_m + \mu_d^A - \Sigma_m^A) \\ &\times (i\omega_m + i\nu_l + \mu_d^B - \Sigma_{m+l}^B) \frac{\frac{F_\infty(\bar{Z}_{m+l})}{\bar{Z}_{m+l}} - \frac{F_\infty(\bar{Z}_m)}{\bar{Z}_m}}{\bar{Z}_m^2 - \bar{Z}_{m+l}^2}, \end{aligned} \quad (36)$$

and

$$\begin{aligned} \frac{1}{N} \sum_{\mathbf{k}} \bar{\gamma}_{\mathbf{k}}^2 G_{\mathbf{k},m}^{AB} G_{\mathbf{k},m+l}^{AB} &= \frac{1}{N} \sum_{\mathbf{k}} \bar{\gamma}_{\mathbf{k}}^2 G_{\mathbf{k},m}^{BA} G_{\mathbf{k},m+l}^{BA} \\ &= \frac{1}{2} \frac{\bar{Z}_{m+l} F_\infty(\bar{Z}_{m+l}) - \bar{Z}_m F_\infty(\bar{Z}_m)}{\bar{Z}_m^2 - \bar{Z}_{m+l}^2}. \end{aligned} \quad (37)$$

Hence, the total expression for the generalized polariza-

tion $\Pi_{m,m+l}$ is

$$\begin{aligned} \Pi_{m,m+l} = \frac{1}{2} \left\{ \frac{F_\infty(\bar{Z}_{m+l}) - F_\infty(\bar{Z}_m)}{\bar{Z}_{m+l} - \bar{Z}_m} \right. \\ \left. \times \left[(i\omega_m + \mu_d^B - \Sigma_m^B)(i\omega_m + i\nu_l + \mu_d^A - \Sigma_{m+l}^A) \right. \right. \\ \left. \left. + (i\omega_m + \mu_d^A - \Sigma_m^A)(i\omega_m + i\nu_l + \mu_d^B - \Sigma_{m+l}^B) \right] \right. \\ \left. + 2 \frac{\bar{Z}_{m+l} F_\infty(\bar{Z}_{m+l}) - \bar{Z}_m F_\infty(\bar{Z}_m)}{\bar{Z}_m^2 - \bar{Z}_{m+l}^2} \right\}. \end{aligned} \quad (38)$$

Then, after substituting this expression for $\Pi_{m,m+l}$ into Eq. (29) and replacing the summation over fermionic Matsubara frequencies by integrals over the real frequency axis, the total expression for the nonresonant response function equals

$$\begin{aligned} \chi_{NB_{1g}}(\Omega) = \frac{1}{4\pi^2} \int_{-\infty}^{+\infty} d\omega [f(\omega) - f(\omega + \Omega)] \\ \times \text{Re} \left\{ \frac{F_\infty^*[\bar{Z}(\omega + \Omega)] - F_\infty[\bar{Z}(\omega)]}{\bar{Z}^*(\omega + \Omega) - \bar{Z}(\omega)} \right. \\ \left. \times \left([\omega + \mu_d^B - \Sigma^B(\omega)][\omega + \Omega + \mu_d^A - \Sigma^{A*}(\omega + \Omega)] \right. \right. \\ \left. \left. + [\omega + \mu_d^A - \Sigma^A(\omega)][\omega + \Omega + \mu_d^B - \Sigma^{B*}(\omega + \Omega)] \right) \right. \\ \left. + 2 \frac{\bar{Z}^*(\omega + \Omega) F_\infty^*[\bar{Z}(\omega + \Omega)] - \bar{Z}(\omega) F_\infty[\bar{Z}(\omega)]}{\bar{Z}^2(\omega) - [\bar{Z}^*(\omega + \Omega)]^2} \right. \\ \left. - \frac{F_\infty[\bar{Z}(\omega + \Omega)] - F_\infty[\bar{Z}(\omega)]}{\bar{Z}^2(\omega) - \bar{Z}^2(\omega + \Omega)} \right. \\ \left. \times \left([\omega + \mu_d^B - \Sigma^B(\omega)][\omega + \Omega + \mu_d^A - \Sigma^A(\omega + \Omega)] \right. \right. \\ \left. \left. + [\omega + \mu_d^A - \Sigma^A(\omega)][\omega + \Omega + \mu_d^B - \Sigma^B(\omega + \Omega)] \right) \right. \\ \left. - 2 \frac{\bar{Z}(\omega + \Omega) F_\infty[\bar{Z}(\omega + \Omega)] - \bar{Z}(\omega) F_\infty[\bar{Z}(\omega)]}{\bar{Z}^2(\omega) - \bar{Z}^2(\omega + \Omega)} \right\}. \end{aligned} \quad (39)$$

One can check that this expression for the Raman response function (for B_{1g} symmetry) in the CDW phase is connected with the one for the optical conductivity³ by the Shastry-Shraiman relation¹²

$$\chi_{NB_{1g}}(\Omega) = \Omega \sigma(\Omega), \quad (40)$$

indicating that this relation continues to hold even in the ordered phases.

The case of A_{1g} symmetry has both terms of the Feynman diagram of Fig. 2 contributing to the expression for the nonresonant response function. According to the

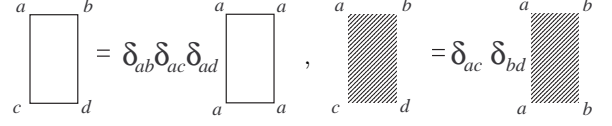


FIG. 3: The irreducible charge vertex becomes local in DMFT and, accordingly, the reducible charge vertex depends only on two sublattice indexes.

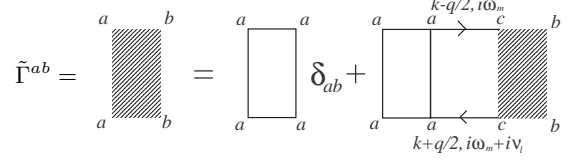


FIG. 4: The Bethe-Salpeter equation for the reducible charge vertex in CDW chessboard phase.

form of the stress-tensor factor, the summation over momentum of the bare loop yields

$$\begin{aligned} \Pi_{m,m+l}^{(1)} = \frac{1}{2} \left\{ \frac{\bar{Z}_{m+l} F_\infty(\bar{Z}_{m+l}) - \bar{Z}_m F_\infty(\bar{Z}_m)}{\bar{Z}_m^2 - \bar{Z}_{m+l}^2} \right. \\ \left. \times \left[(i\omega_m + \mu_d^B - \Sigma_m^B)(i\omega_m + i\nu_l + \mu_d^A - \Sigma_{m+l}^A) \right. \right. \\ \left. \left. + (i\omega_m + \mu_d^A - \Sigma_m^A)(i\omega_m + i\nu_l + \mu_d^B - \Sigma_{m+l}^B) \right] \right. \\ \left. + 1 + \frac{\bar{Z}_{m+l}^3 F_\infty(\bar{Z}_{m+l}) - \bar{Z}_m^3 F_\infty(\bar{Z}_m)}{\bar{Z}_m^2 - \bar{Z}_{m+l}^2} \right\} \end{aligned} \quad (41)$$

which is different from the one for the B_{1g} symmetry in Eq. (38).

The second term of the Feynman diagram in Fig. 1 describes the charge screening effects through the reducible charge vertex, which is defined through the irreducible one. In the DMFT approach, the irreducible charge vertex Γ_a is local and different for different sublattices (see Fig. 3); nevertheless, it has the same functional form as in the uniform phase, which is equal to¹⁶

$$\Gamma_a(i\omega_m, i\omega_{m'}; i\nu_l) = \delta_{mm'} \Gamma_{m,m+l}^a \quad (42)$$

$$\Gamma_{m,m+l}^a = \frac{1}{T} \frac{\Sigma_m^a - \Sigma_{m+l}^a}{G_m^{aa} - G_{m+l}^{aa}}.$$

This expression also follows from the partially integrated Ward identity, derived by Janis¹⁷. Accordingly, the reducible charge vertex in the CDW chessboard phase depends on two sublattice indexes and is defined by the Bethe-Salpeter equation in Fig. 4

$$\tilde{\Gamma}_{\mathbf{q},m,m+l}^{ab} = \delta_{ab} \Gamma_{m,m+l}^a + T \Gamma_{m,m+l}^a \sum_c \chi_{\mathbf{q},m,m+l}^{ac} \tilde{\Gamma}_{\mathbf{q},m,m+l}^{cb}, \quad (43)$$

where we introduce the bare susceptibility

$$\chi_{\mathbf{q},m,m+l}^{ab} = -\frac{1}{N} \sum_{\mathbf{k}} G_{\mathbf{k},m}^{ab} G_{\mathbf{k}+\mathbf{q},m+l}^{ba}. \quad (44)$$

Now, the generalized polarization can be presented in a compact matrix form as follows

$$\begin{aligned} \Pi_{\mathbf{q},m,m+l}^{(2)} &= \frac{1}{N} \sum_{\mathbf{k}} \begin{bmatrix} \tilde{\gamma}_{\mathbf{k}} & \tilde{\gamma}_{\mathbf{k}} \end{bmatrix} \begin{vmatrix} G_{\mathbf{k}-\frac{\mathbf{q}}{2},m}^{AA} & G_{\mathbf{k}+\frac{\mathbf{q}}{2},m+l}^{AB} & G_{\mathbf{k}-\frac{\mathbf{q}}{2},m}^{AB} & G_{\mathbf{k}+\frac{\mathbf{q}}{2},m+l}^{BB} \\ G_{\mathbf{k}-\frac{\mathbf{q}}{2},m}^{BA} & G_{\mathbf{k}+\frac{\mathbf{q}}{2},m+l}^{AA} & G_{\mathbf{k}-\frac{\mathbf{q}}{2},m}^{BB} & G_{\mathbf{k}+\frac{\mathbf{q}}{2},m+l}^{BA} \end{vmatrix} \\ &\times T \begin{vmatrix} \tilde{\Gamma}_{\mathbf{q},m,m+l}^{AA} & \tilde{\Gamma}_{\mathbf{q},m,m+l}^{AB} \\ \tilde{\Gamma}_{\mathbf{q},m,m+l}^{BA} & \tilde{\Gamma}_{\mathbf{q},m,m+l}^{BB} \end{vmatrix} \frac{1}{N} \sum_{\mathbf{k}'} \begin{vmatrix} G_{\mathbf{k}'-\frac{\mathbf{q}}{2},m}^{AA} & G_{\mathbf{k}'+\frac{\mathbf{q}}{2},m+l}^{BA} & G_{\mathbf{k}'-\frac{\mathbf{q}}{2},m}^{AB} & G_{\mathbf{k}'+\frac{\mathbf{q}}{2},m+l}^{AA} \\ G_{\mathbf{k}'-\frac{\mathbf{q}}{2},m}^{BA} & G_{\mathbf{k}'+\frac{\mathbf{q}}{2},m+l}^{BB} & G_{\mathbf{k}'-\frac{\mathbf{q}}{2},m}^{BB} & G_{\mathbf{k}'+\frac{\mathbf{q}}{2},m+l}^{AB} \end{vmatrix} \begin{bmatrix} \tilde{\gamma}_{\mathbf{k}'} \\ \tilde{\gamma}_{\mathbf{k}'} \end{bmatrix}. \end{aligned} \quad (45)$$

The next step is to put $\mathbf{q} = 0$, expand the expression via partial fractions with respect to the band energy $\epsilon_{\mathbf{k}}$ and calculate the sums over momentum \mathbf{k} . After some tedious algebra, we obtain the final expression for $\Pi_{m,m+l}^{(2)}$

$$\begin{aligned} \Pi_{m,m+l}^{(2)} &= \frac{1}{\Delta_{m,m+l}} \frac{[\bar{Z}_{m+l} F_{\infty}(\bar{Z}_{m+l}) - \bar{Z}_m F_{\infty}(\bar{Z}_m)]^2}{\bar{Z}_m^2 - \bar{Z}_{m+l}^2} \\ &\times \left\{ [i(2\omega_m + \nu_l) + 2\mu_d^B - \Sigma_m^B - \Sigma_{m+l}^B] \frac{\Sigma_m^A - \Sigma_{m+l}^A}{G_m^{AA} - G_{m+l}^{AA}} \left([i(2\omega_m + \nu_l) + 2\mu_d^B - \Sigma_m^B - \Sigma_{m+l}^B] \right. \right. \\ &\times \left. \left\{ [\bar{Z}_m^2 - \bar{Z}_{m+l}^2] - (i\omega_m + \mu_d^B - \Sigma_m^B)(i\omega_m + i\nu_l + \mu_d^B - \Sigma_{m+l}^B) \left[\frac{F_{\infty}(\bar{Z}_{m+l})}{\bar{Z}_{m+l}} - \frac{F_{\infty}(\bar{Z}_m)}{\bar{Z}_m} \right] \frac{\Sigma_m^B - \Sigma_{m+l}^B}{G_m^{BB} - G_{m+l}^{BB}} \right\} \right. \\ &+ \left. [i(2\omega_m + \nu_l) + 2\mu_d^A - \Sigma_m^A - \Sigma_{m+l}^A] \frac{\Sigma_m^A - \Sigma_{m+l}^A}{G_m^{AA} - G_{m+l}^{AA}} [\bar{Z}_{m+l} F_{\infty}(\bar{Z}_{m+l}) - \bar{Z}_m F_{\infty}(\bar{Z}_m)] \right) \\ &[i(2\omega_m + \nu_l) + 2\mu_d^A - \Sigma_m^A - \Sigma_{m+l}^A] \frac{\Sigma_m^B - \Sigma_{m+l}^B}{G_m^{BB} - G_{m+l}^{BB}} \left([i(2\omega_m + \nu_l) + 2\mu_d^A - \Sigma_m^A - \Sigma_{m+l}^A] \right. \\ &\times \left. \left\{ [\bar{Z}_m^2 - \bar{Z}_{m+l}^2] - (i\omega_m + \mu_d^A - \Sigma_m^A)(i\omega_m + i\nu_l + \mu_d^A - \Sigma_{m+l}^A) \left[\frac{F_{\infty}(\bar{Z}_{m+l})}{\bar{Z}_{m+l}} - \frac{F_{\infty}(\bar{Z}_m)}{\bar{Z}_m} \right] \frac{\Sigma_m^A - \Sigma_{m+l}^A}{G_m^{AA} - G_{m+l}^{AA}} \right\} \right. \\ &+ \left. [i(2\omega_m + \nu_l) + 2\mu_d^B - \Sigma_m^B - \Sigma_{m+l}^B] \frac{\Sigma_m^B - \Sigma_{m+l}^B}{G_m^{BB} - G_{m+l}^{BB}} [\bar{Z}_{m+l} F_{\infty}(\bar{Z}_{m+l}) - \bar{Z}_m F_{\infty}(\bar{Z}_m)] \right) \left. \right\}, \end{aligned} \quad (46)$$

where

$$\Delta_{m,m+l} = \det \|\delta_{ab} - T\Gamma_{m,m+l}^a \chi_{\mathbf{q}=0,m,m+l}^{ab}\| \quad (47)$$

comes from the solution of the Bethe-Salpeter equation in Eq. (43). Finally, the total expression for the generalized polarization is obtained as the sum of the two contributions

$$\Pi_{m,m+l} = \Pi_{m,m+l}^{(1)} + \Pi_{m,m+l}^{(2)}. \quad (48)$$

Next, we perform an analytical continuation (which is straightforward because we have the appropriate functional forms which allow us to replace Matsubara frequencies by real frequencies) and substitute into Eq. (31) which yields the final expression for the nonresonant Raman response function in the A_{1g} channel. This step

is completely straightforward, so we do not write down the final expressions in terms of integrals over the real frequency.

D. X-ray scattering: $q \neq 0$

In the case of inelastic X-ray scattering, the incident photon exchanges both energy and momentum with the electronic matter. The entire formalism derived for Raman scattering remains the same as described above and there is no need to rewrite it for this case. The only difference is in the summations over momentum. The Feynman diagrams in Fig. 1 together with the Bethe-Salpeter equation in Fig. 4 contain several momentum summa-

tions which can be evaluated separately¹⁸. First, the bare susceptibility in Eq. (44), which enters the Bethe-Salpeter equation for the total charge vertex in Eq. (43), contains the following components

$$\chi_{\mathbf{q},m,m+l}^{AA} = \frac{(i\omega_m + \mu_d^B - \Sigma_m^B)(i\omega_{m+l} + \mu_d^B - \Sigma_{m+l}^B)}{2\bar{Z}_m\bar{Z}_{m+l}} \quad (49)$$

$$\times [\chi_0(\bar{Z}_m, \bar{Z}_{m+l}, \mathbf{q}) - \chi_0(\bar{Z}_m, -\bar{Z}_{m+l}, \mathbf{q})],$$

$$\chi_{\mathbf{q},m,m+l}^{BB} = \frac{(i\omega_m + \mu_d^A - \Sigma_m^A)(i\omega_{m+l} + \mu_d^A - \Sigma_{m+l}^A)}{2\bar{Z}_m\bar{Z}_{m+l}} \quad (50)$$

$$\times [\chi_0(\bar{Z}_m, \bar{Z}_{m+l}, \mathbf{q}) - \chi_0(\bar{Z}_m, -\bar{Z}_{m+l}, \mathbf{q})],$$

and

$$\chi_{\mathbf{q},m,m+l}^{AB} = \chi_{\mathbf{q},m,m+l}^{BA} \quad (51)$$

$$= \frac{1}{2} [\chi_0(\bar{Z}_m, \bar{Z}_{m+l}, \mathbf{q}) + \chi_0(\bar{Z}_m, -\bar{Z}_{m+l}, \mathbf{q})],$$

where

$$\chi_0(\bar{Z}_m, \bar{Z}_{m+l}, \mathbf{q}) = \chi_0(-\bar{Z}_m, -\bar{Z}_{m+l}, \mathbf{q}) \quad (52)$$

$$= -\frac{1}{N} \sum_{\mathbf{k}} \frac{1}{\bar{Z}_m - \epsilon_{\mathbf{k}-\frac{\mathbf{q}}{2}}} \frac{1}{\bar{Z}_{m+l} - \epsilon_{\mathbf{k}+\frac{\mathbf{q}}{2}}}$$

$$= -\frac{1}{\sqrt{1-X^2}} \int_{-\infty}^{+\infty} \frac{d\epsilon}{\bar{Z}_{m+l} - \epsilon} \rho(\epsilon) F_{\infty} \left(\frac{\bar{Z}_m - \epsilon X}{\sqrt{1-X^2}} \right).$$

Here, the function $F_{\infty}(Z)$ is the Hilbert transform of the hypercubic density of states as defined in Eq. (14) and all the transferred momentum dependence is only through the quantity

$$X = \frac{1}{D} \sum_{p=1}^D \cos q_p. \quad (53)$$

The second diagram in Fig. 1 contains summations over \mathbf{k} and \mathbf{k}' which involve stress-tensor amplitudes $\tilde{\gamma}_{\mathbf{k}}$

$$\chi_{\mathbf{q},m,m+l}^a = \frac{1}{N} \sum_{\mathbf{k}} \tilde{\gamma}_{\mathbf{k}} \quad (54)$$

$$\times \left[G_{\mathbf{k}-\frac{\mathbf{q}}{2},m}^{Aa} G_{\mathbf{k}+\frac{\mathbf{q}}{2},m+l}^{aB} + G_{\mathbf{k}-\frac{\mathbf{q}}{2},m}^{Ba} G_{\mathbf{k}+\frac{\mathbf{q}}{2},m+l}^{aA} \right]$$

and there are two different terms:

$$\chi_{\mathbf{q},m,m+l}^A = \frac{i\omega_m + \mu_d^B - \Sigma_m^B}{2\bar{Z}_m} \quad (55)$$

$$\times [\chi_0'(\bar{Z}_m, \bar{Z}_{m+l}, \mathbf{q}) + \chi_0'(\bar{Z}_m, -\bar{Z}_{m+l}, \mathbf{q})]$$

$$+ \frac{i\omega_{m+l} + \mu_d^B - \Sigma_{m+l}^B}{2\bar{Z}_{m+l}}$$

$$\times [\chi_0'(\bar{Z}_m, \bar{Z}_{m+l}, \mathbf{q}) - \chi_0'(\bar{Z}_m, -\bar{Z}_{m+l}, \mathbf{q})]$$

and

$$\chi_{\mathbf{q},m,m+l}^B = \frac{i\omega_m + \mu_d^A - \Sigma_m^A}{2\bar{Z}_m} \quad (56)$$

$$\times [\chi_0'(\bar{Z}_m, \bar{Z}_{m+l}, \mathbf{q}) + \chi_0'(\bar{Z}_m, -\bar{Z}_{m+l}, \mathbf{q})]$$

$$+ \frac{i\omega_{m+l} + \mu_d^A - \Sigma_{m+l}^A}{2\bar{Z}_{m+l}}$$

$$\times [\chi_0'(\bar{Z}_m, \bar{Z}_{m+l}, \mathbf{q}) - \chi_0'(\bar{Z}_m, -\bar{Z}_{m+l}, \mathbf{q})],$$

where

$$\chi_0'(\bar{Z}_m, \bar{Z}_{m+l}, \mathbf{q}) = -\chi_0'(-\bar{Z}_m, -\bar{Z}_{m+l}, \mathbf{q}) \quad (57)$$

$$= -\frac{1}{N} \sum_{\mathbf{k}} \tilde{\gamma}_{\mathbf{k}} \frac{1}{\bar{Z}_m - \epsilon_{\mathbf{k}-\frac{\mathbf{q}}{2}}} \frac{1}{\bar{Z}_{m+l} - \epsilon_{\mathbf{k}+\frac{\mathbf{q}}{2}}}$$

$$= \frac{X'}{1+X} \left\{ [\bar{Z}_m + \bar{Z}_{m+l}] \chi_0(\bar{Z}_m, \bar{Z}_{m+l}, \mathbf{q}) \right.$$

$$\left. + F_{\infty}[\bar{Z}(i\omega_m)] + F_{\infty}[\bar{Z}(i\omega_{m+l})] \right\}.$$

Here the new momentum dependent quantity X' is

$$X' = \frac{1}{D} \sum_{p=1}^D \alpha_p \cos \frac{q_p}{2} \quad (58)$$

with $\alpha_p = 1$ for A_{1g} symmetry and $\alpha_p = (-1)^p$ for B_{1g} symmetry. Now we can find exact expression for the vertex corrections defined by Eq. (45) in the following form

$$\Pi_{\mathbf{q},m,m+l}^{(2)} = \frac{1}{\Delta_{\mathbf{q},m,m+l}} \quad (59)$$

$$\times \left[\chi_{\mathbf{q},m,m+l}^A T\Gamma_{m,m+l}^A \chi_{\mathbf{q},m,m+l}^{AB} T\Gamma_{m,m+l}^B \chi_{\mathbf{q},m,m+l}^B \right.$$

$$+ \chi_{\mathbf{q},m,m+l}^A (1 - T\Gamma_{m,m+l}^B \chi_{\mathbf{q},m,m+l}^{BB}) T\Gamma_{m,m+l}^A \chi_{\mathbf{q},m,m+l}^A$$

$$+ \chi_{\mathbf{q},m,m+l}^B (1 - T\Gamma_{m,m+l}^A \chi_{\mathbf{q},m,m+l}^{AA}) T\Gamma_{m,m+l}^B \chi_{\mathbf{q},m,m+l}^B$$

$$\left. + \chi_{\mathbf{q},m,m+l}^B T\Gamma_{m,m+l}^B \chi_{\mathbf{q},m,m+l}^{BA} T\Gamma_{m,m+l}^A \chi_{\mathbf{q},m,m+l}^A \right],$$

where

$$\Delta_{\mathbf{q},m,m+l} \quad (60)$$

$$= (1 - T\Gamma_{m,m+l}^A \chi_{\mathbf{q},m,m+l}^{AA}) (1 - T\Gamma_{m,m+l}^B \chi_{\mathbf{q},m,m+l}^{BB})$$

$$- T\Gamma_{m,m+l}^A \chi_{\mathbf{q},m,m+l}^{AB} T\Gamma_{m,m+l}^B \chi_{\mathbf{q},m,m+l}^{BA}$$

Finally, the bare loop contribution of the first diagram in Fig. 1 contains summations over momentum \mathbf{k} of the product of two Green functions and the square of the stress-tensor factor. It is equal to

$$\Pi_{\mathbf{q},m,m+l}^{(1)} = \bar{\chi}_0(\bar{Z}_m, \bar{Z}_{m+l}, \mathbf{q}) + \bar{\chi}_0(\bar{Z}_m, -\bar{Z}_{m+l}, \mathbf{q}) \quad (61)$$

$$+ \frac{1}{2\bar{Z}_m\bar{Z}_{m+l}} \left[(i\omega_m + \mu_d^A - \Sigma_m^A)(i\omega_{m+l} + \mu_d^A - \Sigma_{m+l}^A) \right.$$

$$+ (i\omega_m + \mu_d^B - \Sigma_m^B)(i\omega_{m+l} + \mu_d^B - \Sigma_{m+l}^B) \left. \right]$$

$$\times [\bar{\chi}_0(\bar{Z}_m, \bar{Z}_{m+l}, \mathbf{q}) - \bar{\chi}_0(\bar{Z}_m, -\bar{Z}_{m+l}, \mathbf{q})]$$

and expressed in terms of χ_0 as follows

$$\begin{aligned}
\bar{\chi}_0(\bar{Z}_m, \bar{Z}_{m+l}, \mathbf{q}) &= \bar{\chi}_0(-\bar{Z}_m, -\bar{Z}_{m+l}, \mathbf{q}) \\
&= -\frac{1}{N} \sum_{\mathbf{k}} \tilde{\gamma}_{\mathbf{k}}^2 \frac{1}{\bar{Z}_m - \epsilon_{\mathbf{k}-\frac{\mathbf{q}}{2}}} \frac{1}{\bar{Z}_{m+l} - \epsilon_{\mathbf{k}+\frac{\mathbf{q}}{2}}} \\
&= \chi_0(\bar{Z}_m, \bar{Z}_{m+l}, \mathbf{q}) \left\{ \frac{t^{*2}}{2} - \frac{t^{*2} X'^2}{1+X} + \frac{[\bar{Z}_m + \bar{Z}_{m+l}]^2 X'^2}{(1+X)^2} \right\} \\
&+ \frac{X'^2}{(1+X)^2} [\bar{Z}_m + \bar{Z}_{m+l}] \{F_\infty[\bar{Z}(i\omega_m)] + F_\infty[\bar{Z}(i\omega_{m+l})]\} \\
&+ \frac{X'^2}{1+X} \{ \bar{Z}_m F_\infty[\bar{Z}(i\omega_m)] + \bar{Z}_{m+l} F_\infty[\bar{Z}(i\omega_{m+l})] - 2 \}.
\end{aligned} \tag{62}$$

The expressions for χ'_0 and $\bar{\chi}_0$ derived above appear to be different from the ones given in Ref. 18. In fact, they are identical (but require some significant algebra to show this); the forms presented above are more convenient for numerical calculations.

In contrast to B_{1g} Raman scattering at $\mathbf{q} = 0$ which is determined only by the bare loop contributions (Fig. 2), in the case of inelastic X-ray scattering, we have both terms contributing for all symmetry channels. The different symmetry channels are distinguished only by the different X' factors, and, as a result, different χ'_0 and $\bar{\chi}_0$ functions. All further numerical calculations are performed by exploiting these three quantities, but the total scheme remains the same. As a result, the generalized polarization in Eq. (59) is described in terms of the χ_0 , χ'_0 and $\bar{\chi}_0$ functions and applying further analytic continuation to the real axis one can obtain the nonresonant inelastic X-ray scattering response functions. The final expressions are too long to be presented here.

E. Nonresonant inelastic X-ray scattering sum rule

The sum rule for the nonresonant inelastic scattering response function is as follows:^{19,20}

$$I = \int_0^{+\infty} d\Omega \Omega \chi_N(\Omega) = \frac{\pi}{2} \langle [\tilde{\gamma}^\dagger(\mathbf{q}) [H, \tilde{\gamma}(\mathbf{q})]] \rangle, \tag{63}$$

where for the case of CDW ordering

$$\begin{aligned}
\tilde{\gamma}(\mathbf{q}) &= \sum_{ab} \sum_{ij} t_{ij}^{ab} e^{i\mathbf{Q}(\mathbf{R}_i^a - \mathbf{R}_j^b)} e^{-i\frac{\mathbf{q}}{2}(\mathbf{R}_i^a + \mathbf{R}_j^b)} \hat{d}_{ia}^\dagger \hat{d}_{jb}, \\
\tilde{\gamma}^\dagger(\mathbf{q}) &= \sum_{ab} \sum_{ij} t_{ji}^{ba} e^{i\mathbf{Q}(\mathbf{R}_j^b - \mathbf{R}_i^a)} e^{i\frac{\mathbf{q}}{2}(\mathbf{R}_i^a + \mathbf{R}_j^b)} \hat{d}_{jb}^\dagger \hat{d}_{ia},
\end{aligned} \tag{64}$$

and momentum \mathbf{Q} determines the symmetry channels

$$\mathbf{Q} = \begin{cases} 0 & \text{for } A_{1g} \\ (\pi, 0, \pi, 0, \dots) & \text{for } B_{1g} \end{cases}. \tag{65}$$

After calculating all required commutators, taking the large dimensional limit, and performing some cumbersome transformations (see the Appendix), we obtain a

sum rule (first moment of the nonresonant inelastic X-ray scattering response function) which contains two contributions

$$I = I_K + I_\Pi. \tag{66}$$

The first contribution comes from the kinetic energy term

$$\begin{aligned}
I_K &= 2(1-X) \int_{-\infty}^{+\infty} d\omega f(\omega) \text{Im} \left\{ \frac{t^{*2}}{2} [\bar{Z}(\omega) F_\infty[\bar{Z}(\omega)] - 1] \right. \\
&\quad \left. - X'^2 \left(\left[\frac{3t^{*2}}{2} - \bar{Z}^2(\omega) \right] [\bar{Z}(\omega) F_\infty[\bar{Z}(\omega)] - 1] + \frac{t^{*2}}{2} \right) \right\}
\end{aligned} \tag{67}$$

and is similar to the one in the uniform case.¹⁹ The other one originates from the potential energy term and satisfies

$$\begin{aligned}
I_\Pi &= \int_{-\infty}^{+\infty} d\omega f(\omega) \text{Im} \left\{ \sum_a [\Sigma^a(\omega) - U n_f^a] \right. \\
&\quad \times \left[\frac{t^{*2}}{2} (1 - X'^2) G^{aa}(\omega) + X'^2 \lambda^a(\omega) \right] \\
&\quad \left. + X'^2 [\bar{Z}(\omega) F_\infty[\bar{Z}(\omega)] - 1] [\Sigma^A(\omega) - \Sigma^B(\omega)]^2 \right\} \\
&\quad - \frac{\pi}{2} U t^{*2} (1 - X'^2) (n_f^A - n_f^B) (n_d^A - n_d^B).
\end{aligned} \tag{68}$$

The first contribution in braces has the same shape as the potential energy contribution of the sum rule in the uniform phase.¹⁹ The other terms appear only in the CDW phase and are proportional to the square of the CDW order parameter $(\Delta n_f)^2$.

By examining different points in the Brillouin zone (BZ), one can extract information regarding the potential and kinetic-energy contributions. For instance, in the case of Raman scattering ($\mathbf{q} = 0$, $X = 1$) we have contributions only from the potential-energy term ($I_K = 0$), which are different for the A_{1g} symmetry ($X' = 1$)

$$\begin{aligned}
I_\Pi &= \int_{-\infty}^{+\infty} d\omega f(\omega) \text{Im} \left\{ \sum_a [\Sigma^a(\omega) - U n_f^a] \lambda^a(\omega) \right. \\
&\quad \left. + [\bar{Z}(\omega) F_\infty[\bar{Z}(\omega)] - 1] [\Sigma^A(\omega) - \Sigma^B(\omega)]^2 \right\},
\end{aligned} \tag{69}$$

and for the B_{1g} symmetry ($X' = 0$)

$$\begin{aligned}
I_\Pi &= \int_{-\infty}^{+\infty} d\omega f(\omega) \text{Im} \left\{ \sum_a [\Sigma^a(\omega) - U n_f^a] \frac{t^{*2}}{2} G^{aa}(\omega) \right\} \\
&\quad - \frac{\pi}{2} U t^{*2} (n_f^A - n_f^B) (n_d^A - n_d^B).
\end{aligned} \tag{70}$$

For other points in the BZ (inelastic X-ray scattering), we have contributions from both the kinetic and potential-energy terms. For instance, for the case of B_{1g} symmetry along the BZ-diagonal [$\mathbf{q} = (q, q, q, q, \dots)$, $-1 \leq X \leq 1$, $X' = 0$] and for all symmetry channels at the BZ corner [$\mathbf{q} = (\frac{\pi}{a}, \frac{\pi}{a}, \frac{\pi}{a}, \frac{\pi}{a}, \dots)$, $X = -1$, $X' = 0$] we have:

$$I_K = 2(1 - X) \int_{-\infty}^{+\infty} d\omega f(\omega) \text{Im} \left\{ \frac{t^{*2}}{2} [\bar{Z}(\omega) F_{\infty}[\bar{Z}(\omega)] - 1] \right\}, \quad (71)$$

$$I_{\Pi} = \int_{-\infty}^{+\infty} d\omega f(\omega) \text{Im} \left\{ \sum_a [\Sigma^a(\omega) - U n_f^a] \frac{t^{*2}}{2} G^{aa}(\omega) \right\} \\ - \frac{\pi}{2} U t^{*2} (n_f^A - n_f^B) (n_d^A - n_d^B).$$

One can see, that in this case the kinetic-energy contribution is equal (up to an overall constant) to the average kinetic energy which also enters the sum rule for optical conductivity.³

III. NUMERICAL RESULTS

We begin with an analysis of nonresonant Raman scattering in the CDW phase. We present results for the cases of a dirty metal with $U = 0.5$ (Fig. 5), a near critical Mott insulator with $U = 1.5$ (Fig. 6), and a moderate gap Mott insulator with $U = 2.5$ (Fig. 7).

In Fig. 5, we plot the Raman response function for different temperatures in the case of a dirty metal with $U = 0.5$. At temperatures higher than the critical order, we see the expected behavior for a dirty metal: namely, there is a peak at low energy and a spread on the order of the metallic bandwidth. The system does not have a low energy Fermi-liquid peak, because it is not a Fermi liquid. Below the critical temperature, when the CDW gap arises, the shape of the response function changes significantly. The main peak is shifted to higher frequency at $\Omega \approx U$, which corresponds to transitions between the lowest band at $\omega \leq -U/2$ and the upper band at $\omega \geq U/2$ (see the DOS in Ref. 3). Two additional peaks at lower frequencies correspond to the transitions from the upper and lower bands onto the subgap states and between the subgap states (which are present for a wide range of temperatures below T_c but above $T = 0$). Because the subgap DOS vanishes at $T = 0$, these peaks must vanish with $T \rightarrow 0$. In panel (a), we plot the nonresonant response function for the B_{1g} symmetry. In this symmetry channel, there is a sharp main peak with a square root singularity at $T = 0$. This behavior was already seen in the optical conductivity³, and follows for the Raman scattering directly from the Shastry-Shraiman relation in Eq. (40). For the A_{1g} channel, as plotted in panel (b), the response is much smaller

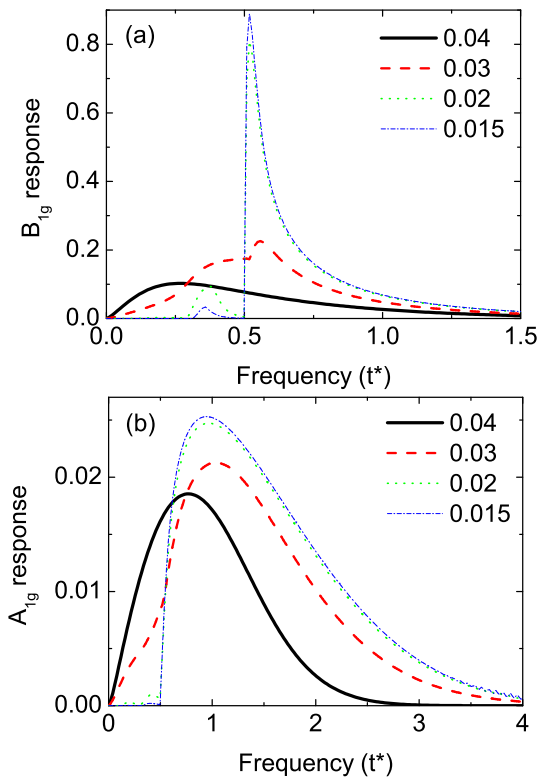


FIG. 5: (Color online) Nonresonant Raman response function for the two symmetry channels [(a) being the B_{1g} channel and (b) being the A_{1g} channel] in a dirty metal with $U = 0.5$. The set of curves corresponds to a range of temperatures from the uniform to the ordered phase ($T_c \approx 0.034$).

and smooth (without sharp singularities) due to the effects of the dynamical charge screening. Note how the overall scale of the response function is much smaller, and how there are no remnants of the sharp singularity seen in the B_{1g} channel. Because the A_{1g} channel has the same symmetry as the lattice, we expect the screening effects to be significant here, and to be the strongest at low frequencies. This can also be seen in the figure.

In Fig. 6, we plot the results for a near-critical Mott insulator with $U = 1.5$. The basic results remain quite similar to the metallic case. We see the response function change dramatically as the system orders, with complex behavior at low temperature and low energy due to the subgap states, and then finally leading to the square root singularity in the B_{1g} channel and smoother behavior in the A_{1g} channel, with no singularity, and significantly reduced spectral weight. The main change is the energy scale, since the gap is always identically equal to U at $T = 0$, and this is reflected in the “pushing” of the spectra to the right. As we go from a near-gap insulator to a moderate-gap insulator with $U = 2.5$ (Fig. 7), we once again see similar kinds of behavior. In particular, we observe three peaks: the main CDW-gap peak at $\Omega = U$ is sharp for the B_{1g} symmetry in panel (a) and smoothed for the A_{1g} symmetry in panel (b) and the two low-energy

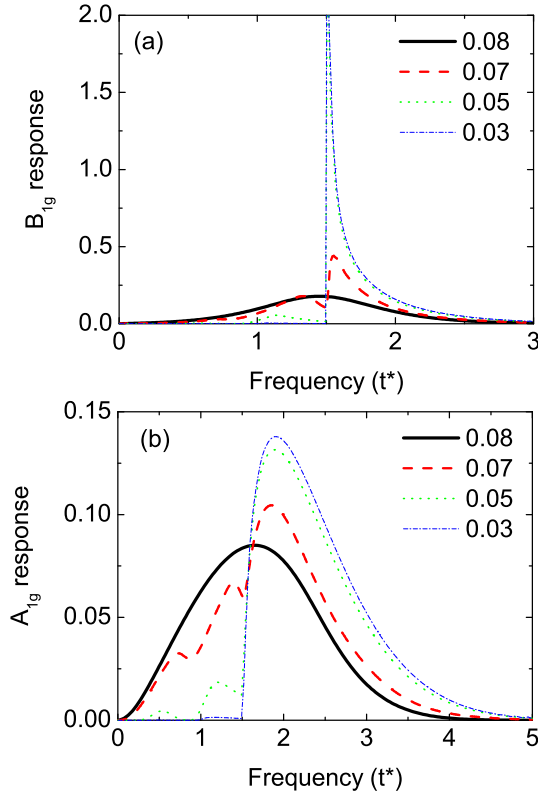


FIG. 6: (Color online) Nonresonant Raman response function for the two symmetry channels in a near critical Mott insulator with $U = 1.5$. The set of curves corresponds to a range of temperatures from the uniform to the ordered phase ($T_c \approx 0.075$).

peaks have strong temperature dependence.

For nonresonant inelastic X-ray scattering, we investigate the behavior of the response functions for the different transferred momentum values \mathbf{q} in the first Brillouin zone (BZ). Because all the momentum dependence enters only through the parameters X and X' , we must first understand their behavior in the BZ. We want our results to make contact with real physical systems, like a two-dimensional system, so we choose the following paths in the first BZ: the zone diagonal (zd) path lies in the so-called Σ -direction with $\mathbf{q} = (q, q, q, q, \dots)$ and $-1 \leq X \leq 1$; the zone edge (ze) path lies in the Z -direction with $\mathbf{q} = (\frac{\pi}{a}, q, \frac{\pi}{a}, q, \dots)$ and $-1 \leq X \leq 0$, and then continues along the zone edge path in the Δ -direction with $\mathbf{q} = (q, 0, q, 0, \dots)$ and $0 \leq X \leq 1$. These results are depicted in Fig. 8. The corresponding dependence of X and X' along these paths are plotted in Fig. 9. One can see, that along the Z -direction, the X' value and, as a result, the response functions, are the same in both symmetry channels. For other directions, they are different. In addition, $X' = 0$ along the zone diagonal Σ -direction for the B_{1g} symmetry and the corresponding response function is determined only by the bare contributions with no vertex corrections entering.

Having established the values of X and X' that we are

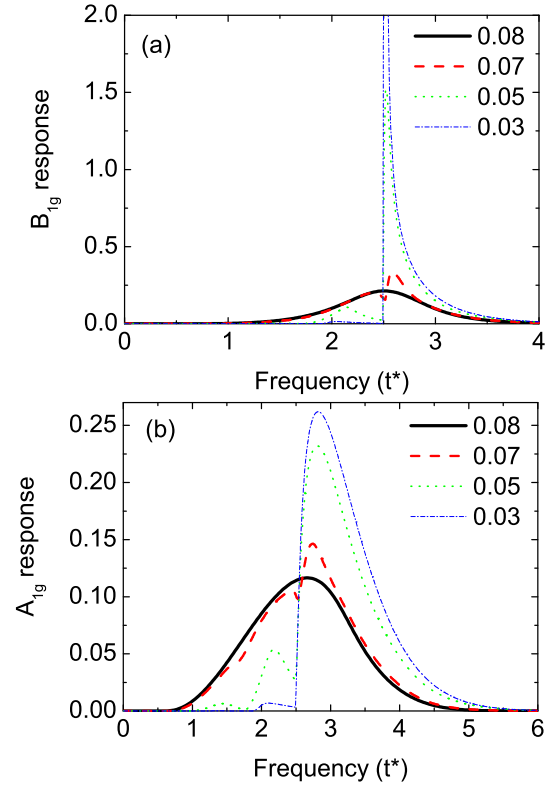


FIG. 7: (Color online) Nonresonant Raman response function for the two symmetry channels in a moderate gap Mott insulator with $U = 2.5$. The set of curves corresponds to a range of temperatures from the uniform to the ordered phase ($T_c \approx 0.072$).

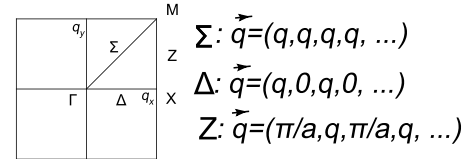


FIG. 8: Schematic of the first Brillouin zone with the high symmetry points labeled. Although we work in infinite dimensions, we are trying to make contact with the two-dimensional BZ.

using, we now show our numerical calculations of the nonresonant inelastic X-ray response functions for the case of a dirty metal with $U = 0.5$ at different temperatures and transferred momentum. In Fig. 10, we present results for the B_{1g} symmetry and in Fig. 11 for the A_{1g} symmetry. At the zone center ($X = 1$), the response is the Raman scattering (see figures above) with sharp features in the B_{1g} channel and with strong screening in the A_{1g} channel. When we move away of the zone center, first of all, the sharp square root singularity at $\Omega = U$ in the B_{1g} channel is rapidly replaced by a step like behavior with a strong enhancement at the Brillouin zone corner $X = -1$, when the transferred momentum coincides with the CDW wave vector. For the A_{1g} sym-

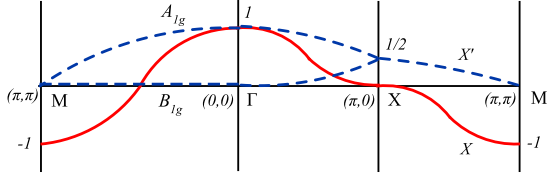


FIG. 9: Plot of X and X' along the zone diagonal path and zone edge path in the first Brillouin zone.

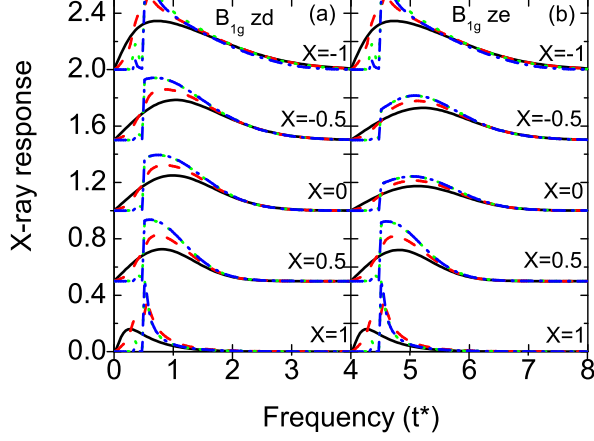


FIG. 10: Nonresonant X-ray scattering response function in the B_{1g} channel for $U = 0.5$ along the zone diagonal and zone edge of the first Brillouin zone. The set of curves correspond to temperatures $T = 0.04, 0.03, 0.02, 0.015$.

metry, we have a different scenario: there is a continuous enhancement without any sharp features, when we move along the zone diagonal and there is a continuous development of a step-like feature, when we move along the zone edge with a strong enhancement at the zone corner, because the screening due to the vertex corrections van-

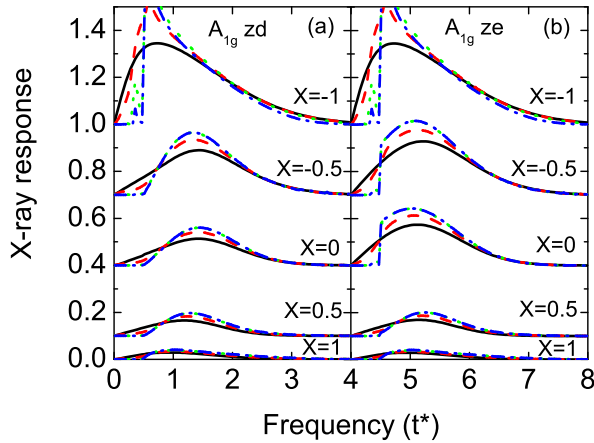


FIG. 11: Nonresonant X-ray scattering response function in the A_{1g} channel for $U = 0.5$ along the zone diagonal and zone edge of the first Brillouin zone. The set of curves correspond to temperatures $T = 0.04, 0.03, 0.02, 0.015$.

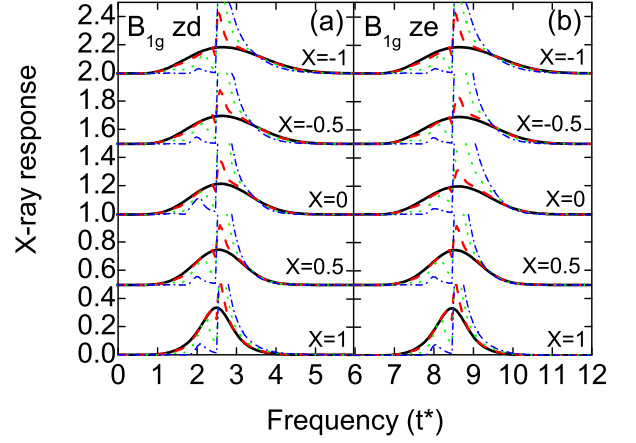


FIG. 12: Nonresonant inelastic X-ray scattering response function in the B_{1g} channel for $U = 2.5$ along the zone diagonal and the zone edge of the first BZ. The set of curves corresponds to the temperatures $T = 0.08, 0.07, 0.06, 0.04$.

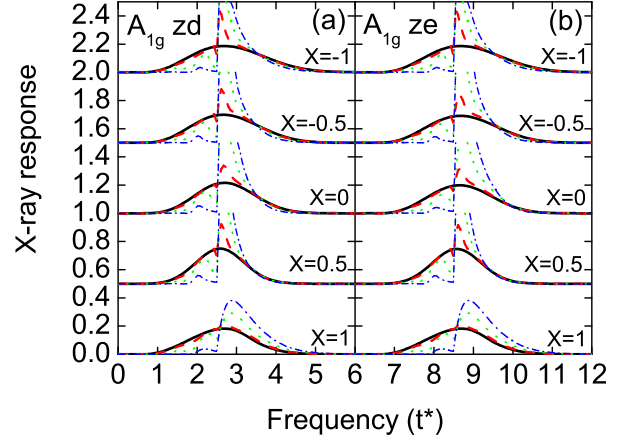


FIG. 13: Nonresonant inelastic X-ray scattering response function in the A_{1g} channel for $U = 2.5$ along the zone diagonal and the zone edge of the first BZ. The set of curves corresponds to the temperatures $T = 0.08, 0.07, 0.06, 0.04$.

ishes there (since the B_{1g} and A_{1g} response functions are identical and have no vertex corrections there). In both cases, there is a large enhancement of the scattering response function as we move from the zone center to the zone corner. This is due, in part, to the fact that the screening is much more effective at the zone center for the A_{1g} channel.

Because the results for the near critical Mott insulator with $U = 1.5$ are similar to the results for the other two U values, we don't show them here. But, we do plot the results for a small gap Mott insulator, with $U = 2.5$ in Figs. 12 and 13). Here, we continue to see similar behavior to what is seen for $U = 0.5$, namely, the character of the response changes rapidly as we move away from the zone-center, the differentiation of the results for different

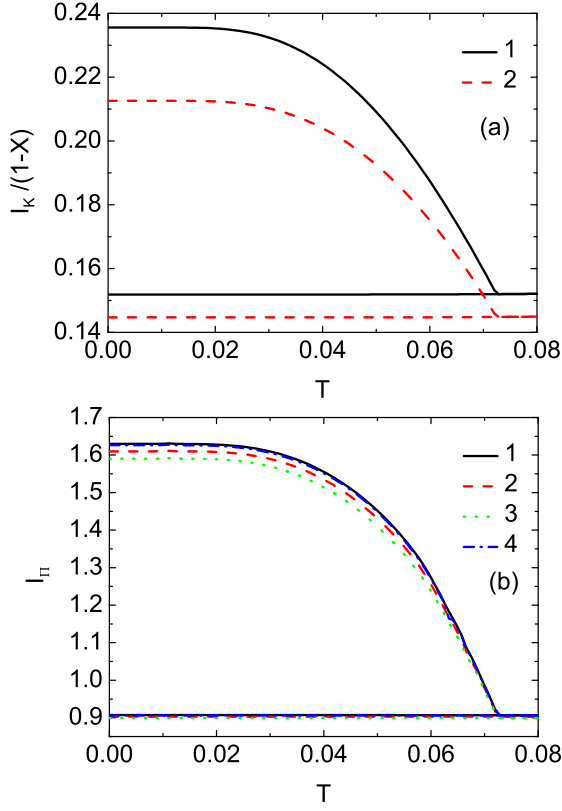


FIG. 14: B_{1g} sum rules as a function of temperature for $U = 2.5$. (a) The kinetic-energy contribution $I_K/(1-X)$: 1 — zone-diagonal Σ -direction ($-1 \leq X \leq 1$, $X' = 0$); 2 — X -point at zone-edge ($X = 0$). (b) The potential-energy contribution I_{II} : 1 — zone-diagonal Σ -direction ($-1 \leq X \leq 1$, $X' = 0$); 2 — zone-edge $X = -0.5$; 3 — zone-edge $X = 0$ (X -point); 4 — zone-edge $X = 0.5$. The thin lines correspond to the uniform solution artificially continued below T_c .

symmetry channels is reduced, and the results coincide at the zone corner. We also see an enhancement of the signal and a generic broadening of the peaks as we move from the zone center to the zone corner.

Since we have derived first-moment sum rules for all of the response functions, we checked our numerical results by integrating the first moment of the response function and comparing that answer to the results of the moment sum rule expectation values, which are evaluated on the imaginary axis. In all cases we examined, we achieved essentially perfect agreement, with errors less than 0.1%, and arising primarily from the discretization we used in our frequency grid for the numerical integrations.

But the sum rules can actually tell us more about the system. One of the hallmarks of the f -sum rule for the optical conductivity is that the sum rule is fixed and does not change with temperature or interaction strength, so spectral weight is never lost or gained. In a projected low-energy model, this result no longer holds, and the low-energy spectral weight can change with temperature or U , but, as is often the case, the changes are quite

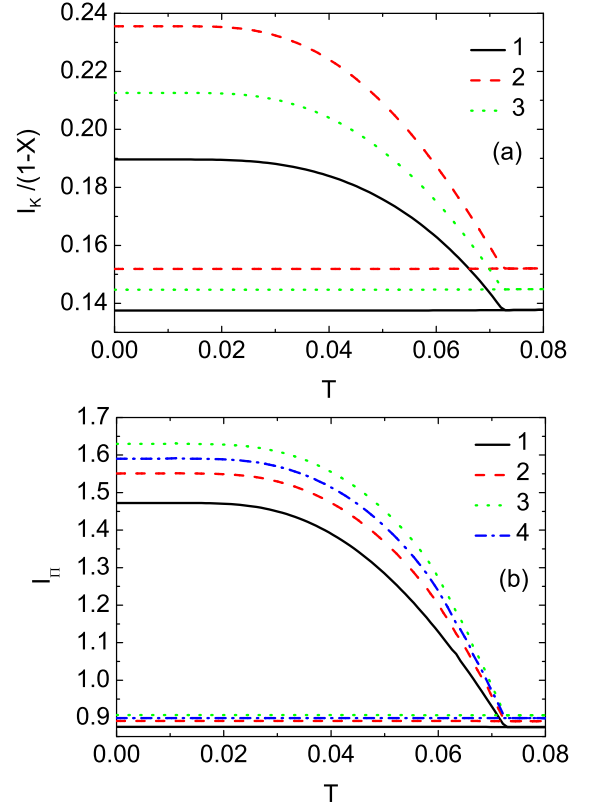


FIG. 15: A_{1g} sum rules as a function of temperature for $U = 2.5$. (a) The kinetic-energy contribution $I_K/(1-X)$: 1 — zone-diagonal $X = 0$; 2 — M -point at zone-corner ($X = -1$); 3 — X -point at zone-edge ($X = 0$). (b) The potential-energy contribution I_{II} : 1 — Γ -point at BZ center ($X = 1$); 2 — zone-diagonal $X = 0$; 3 — BZ corner $X = -1$ (M -point); 4 — zone-edge $X = 0$ (X -point). The thin lines correspond to the uniform solution artificially continued below T_c .

small at low temperature. We can of course investigate this for our system in the CDW phase, by examining how the sum rule evolves for different parameters. We begin with a plot the sum rule for the case of strongly correlated insulator $U = 2.5$ in the B_{1g} channel in Fig. 14 and for the A_{1g} channel in Fig. 15. One can see, that for such values of Coulomb interaction the main contribution to the sum rule comes from the potential-energy part. The momentum dependence of the sum rule in the B_{1g} channel is weak for the potential-energy contribution and strong for the kinetic-energy one [notice the $1-X$ factor in Eq. (67)]. For the A_{1g} channel, both contributions have strong momentum dependence. For both symmetries, the largest values of the sum rule (total and for each contribution) are observed at the BZ corner M -point ($X = -1$) in both the uniform phase and the CDW phase, as could have been guessed due to the enhancement of the overall spectral functions we observed above. The increase in the sum rule below T_c is linear in $T_c - T$ and proportional to the square of the CDW order parameter $(\Delta n_f)^2$. For small values of U (see Figs. 16 and 17),

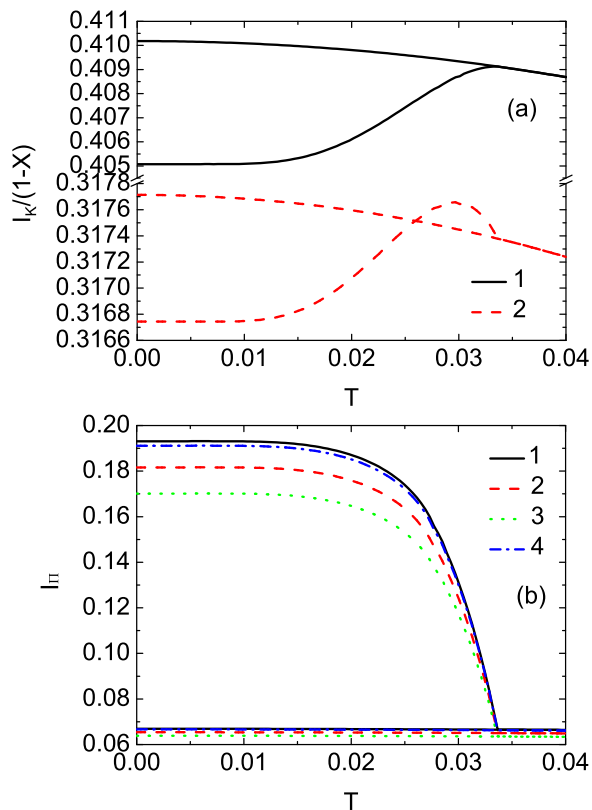


FIG. 16: B_{1g} sum rules as a function of temperature for $U = 0.5$ (we plot the same cases as in Fig. 14).

the kinetic-energy contribution gives the main contribution into the total sum rule. The kinetic-energy contribution continues to display strong momentum dependence and for some momentum its temperature dependence becomes quite nonlinear below T_c , as we already saw for the optical sum rule.³

IV. CONCLUSIONS

In this work, we developed the formalism for nonresonant inelastic Raman and X-ray scattering in the case when the system develops CDW order at low temperature. The formalism is a straightforward generalization of the results in the paramagnetic phase, but requires a careful accounting of the different sublattices and how they enter into the diagrammatic expansions. We also derived first-moment sum rules for these spectra and related the sum rules to different expectation values that can be immediately calculated. We find that the sum rules relate to the potential energy in some cases, while in other cases, both the kinetic energy and the potential energy terms enter into the expectation values.

The main result that we find, is that there is very strong temperature dependence that sets in once we pass through T_c . This occurs because the system rapidly depletes subgap states as it forms the CDW gap, and then

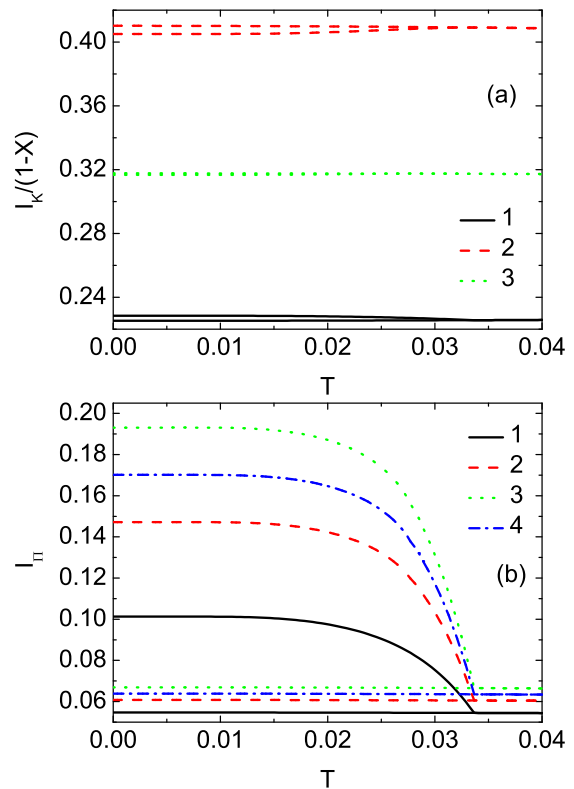


FIG. 17: A_{1g} sum rules as a function of temperature for $U = 0.5$ (we plot the same cases as in Fig. 15).

develops a square-root singularity due to the pile-up of states at $T = 0$. These features can be immediately seen in the light scattering response functions. When vertex corrections act to screen the light scattering, the square root singularity is suppressed, as is the overall magnitude of the light scattering signal. While we see an enhancement of the response, a broadening of the spectra, and an increase in the magnitude of the sum rule as we move from the zone center to the zone corner, we do not see any dramatic behavior associated with the fact that we can transfer momenta that is equal to the ordering wavevector of the CDW. This turns out to be similar to what was seen in the dynamical charge susceptibility of the model as one approached T_c from above¹⁶, and may be related to the fact that the Falicov-Kimball model has a reducible charge vertex that assumes very different behavior for dynamical charge fluctuations as it does for static charge fluctuations, which give rise to the underlying CDW order.

We believe our results will be most relevant to electronic Raman or X-ray scattering on CDW ordered systems in three dimensions. So far, most of the Raman scattering work has focused on understanding how phonons behave as one passes through the transition, including the behavior of the phonon softening for the CDW mode²¹. We hope that our results will inspire experimental groups to also consider examining electronic Raman scattering in CDW systems to see whether they

display the kinds of features that we showed here.

In the future, we will generalize the resonant light scattering results to the CDW phase and examine what modifications enter into the response functions in that case.

Acknowledgments

This publication is based on work supported by Award No. UKP2-2697-LV-06 of the U.S. Civilian Research & Development Foundation (CRDF). J. K. F. acknowledges support from the Department of Energy, Office of Basic Science, under grant number DE-FG02-08ER46542.

APPENDIX: SUM RULE DERIVATION

In this appendix, we present details for the derivation of the first-moment sum rules of inelastic light and X-ray

scattering in the ordered CDW phase. To begin, we must evaluate the first commutator in Eq. (63) which yields

$$\begin{aligned}
[H, \tilde{\gamma}(\mathbf{q})] &= U \sum_{ija} t_{ij}^{a\bar{a}} e^{i\mathbf{Q}(\mathbf{R}_i - \mathbf{R}_j)} e^{-i\frac{\mathbf{q}}{2}(\mathbf{R}_i + \mathbf{R}_j)} \quad (\text{A.1}) \\
&\times (\hat{n}_{if}^a - \hat{n}_{jf}^{\bar{a}}) \hat{d}_{ia}^\dagger \hat{d}_{j\bar{a}} \\
&- \sum_{ijla} t_{il}^{a\bar{a}} t_{lj}^{\bar{a}a} \left[e^{i\mathbf{Q}(\mathbf{R}_i^{\bar{a}} - \mathbf{R}_j^a)} e^{-i\frac{\mathbf{q}}{2}(\mathbf{R}_i^{\bar{a}} + \mathbf{R}_j^a)} \right. \\
&\left. - e^{i\mathbf{Q}(\mathbf{R}_i^a - \mathbf{R}_j^{\bar{a}})} e^{-i\frac{\mathbf{q}}{2}(\mathbf{R}_i^a + \mathbf{R}_j^{\bar{a}})} \right] \hat{d}_{ia}^\dagger \hat{d}_{ja}.
\end{aligned}$$

Here we introduce the notations $\bar{A} = B$ and $\bar{B} = A$ and use the fact that the hopping integral connects only sites which belong to different sublattices.

The second commutator now gives

$$\begin{aligned}
[\gamma^\dagger(\mathbf{q}) [H, \tilde{\gamma}(\mathbf{q})]] &= U \sum_{ijla} t_{il}^{a\bar{a}} t_{lj}^{\bar{a}a} e^{i\mathbf{Q}(\mathbf{R}_i - \mathbf{R}_j)} \left[e^{i\frac{\mathbf{q}}{2}(\mathbf{R}_i - \mathbf{R}_j)} (\hat{n}_{if}^{\bar{a}} - \hat{n}_{jf}^a) - e^{-i\frac{\mathbf{q}}{2}(\mathbf{R}_i - \mathbf{R}_j)} (\hat{n}_{if}^a - \hat{n}_{jf}^{\bar{a}}) \right] \hat{d}_{ia}^\dagger \hat{d}_{ja} \quad (\text{A.2}) \\
&- \sum_{ijlna} t_{il}^{a\bar{a}} t_{ln}^{\bar{a}a} t_{nj}^{a\bar{a}} \left[e^{i\mathbf{Q}(\mathbf{R}_i^a - \mathbf{R}_l^{\bar{a}} + \mathbf{R}_n^a - \mathbf{R}_j^{\bar{a}})} e^{i\frac{\mathbf{q}}{2}(\mathbf{R}_i^a + \mathbf{R}_l^{\bar{a}} - \mathbf{R}_n^a - \mathbf{R}_j^{\bar{a}})} - e^{i\mathbf{Q}(\mathbf{R}_i^a - \mathbf{R}_n^a)} e^{i\frac{\mathbf{q}}{2}(\mathbf{R}_i^a - \mathbf{R}_n^a)} \right. \\
&\left. + e^{i\mathbf{Q}(\mathbf{R}_i^a - \mathbf{R}_l^{\bar{a}} + \mathbf{R}_n^a - \mathbf{R}_j^{\bar{a}})} e^{-i\frac{\mathbf{q}}{2}(\mathbf{R}_i^a + \mathbf{R}_l^{\bar{a}} - \mathbf{R}_n^a - \mathbf{R}_j^{\bar{a}})} - e^{i\mathbf{Q}(\mathbf{R}_i^{\bar{a}} - \mathbf{R}_j^a)} e^{-i\frac{\mathbf{q}}{2}(\mathbf{R}_i^{\bar{a}} - \mathbf{R}_j^a)} \right] \hat{d}_{ia}^\dagger \hat{d}_{j\bar{a}}.
\end{aligned}$$

Next, we use the fact that the hopping is allowed only between NN sites, and we replace $j = i + \delta$ in t_{ij}^{ab} , where δ runs over all of the NNs of site i , to obtain

$$\begin{aligned}
\langle [\gamma^\dagger(\mathbf{q}) [H, \tilde{\gamma}(\mathbf{q})]] \rangle &= Ut^2 \sum_{i\delta\delta'a} e^{-i\mathbf{Q}(\delta+\delta')} \left\langle \left[e^{-i\frac{\mathbf{q}}{2}(\delta+\delta')} (\hat{n}_{i+\delta,f}^{\bar{a}} - \hat{n}_{i+\delta+\delta',f}^a) - e^{i\frac{\mathbf{q}}{2}(\delta+\delta')} (\hat{n}_{i,f}^a - \hat{n}_{i+\delta,f}^{\bar{a}}) \right] \hat{d}_{i,a}^\dagger \hat{d}_{i+\delta+\delta',a} \right\rangle \quad (\text{A.3}) \\
&- t^3 \sum_{i\delta\delta'\delta''a} e^{-i\mathbf{Q}(\delta'+\delta'')} \left[e^{-i\frac{\mathbf{q}}{2}(\delta'+\delta'')} (e^{-i\mathbf{q}\delta} - 1) + e^{i\frac{\mathbf{q}}{2}(\delta'+\delta'')} (e^{i\mathbf{q}\delta} - 1) \right] \left\langle \hat{d}_{i,a}^\dagger \hat{d}_{i+\delta+\delta'+\delta'',a} \right\rangle.
\end{aligned}$$

The first term contains expectation values of three operator products which can be calculated by introducing an auxiliary field $\mu_f^c \rightarrow \mu_f^c + \delta\mu_{l,f}^c$ at site l into the Hamiltonian and taking a functional derivative

$$\langle \hat{d}_{jb}^\dagger \hat{d}_{ia} \hat{n}_{l,f}^c \rangle = T \sum_m \left[T \frac{\delta G_{ij}^{ab}(i\omega_m)}{\delta \mu_{l,f}^c} + n_{l,f}^c G_{ij}^{ab}(i\omega_m) \right] = T \sum_m \left[G_{il}^{ac}(i\omega_m) T \frac{\delta \Sigma_l^c(i\omega_m)}{\delta \mu_{l,f}^c} G_{lj}^{cb}(i\omega_m) + n_{l,f}^c G_{ij}^{ab}(i\omega_m) \right]. \quad (\text{A.4})$$

One can immediately calculate the derivative

$$T \frac{\delta \Sigma_l^c(i\omega_m)}{\delta \mu_{l,f}^c} = \frac{1}{(G_m^c)^2} \frac{Un_f^c(1 - n_f^c)}{(i\omega_m + \mu_d^c - \lambda_m^c)(i\omega_m + \mu_d^c - \lambda_m^c - U)} = \frac{\Sigma_m^c - Un_f^c}{UG_m^c} \quad (\text{A.5})$$

from the solution of the single-impurity problem. After substituting this result into Eq. (A.3), we find that

$$\begin{aligned}
I = & -\frac{\pi T}{2} \sum_m \sum_a \frac{1}{N} \sum_{\mathbf{k}} G_{\mathbf{k}}^{\bar{a}a}(i\omega_m) \left[\epsilon_{\mathbf{k}-\frac{\mathbf{q}}{2}-\mathbf{Q}}^2 (\epsilon_{\mathbf{k}-\mathbf{q}} - \epsilon_{\mathbf{k}}) + \epsilon_{\mathbf{k}+\frac{\mathbf{q}}{2}-\mathbf{Q}}^2 (\epsilon_{\mathbf{k}+\mathbf{q}} - \epsilon_{\mathbf{k}}) \right] \\
& + \frac{\pi T}{2} \sum_m \sum_a \frac{\Sigma_m^a - U n_f^a}{G_m^a} \left\{ \frac{1}{N} \sum_{\mathbf{k}} G_{\mathbf{k}}^{\bar{a}a}(i\omega_m) \epsilon_{\mathbf{k}-\frac{\mathbf{q}}{2}-\mathbf{Q}} \frac{1}{N} \sum_{\mathbf{k}'} G_{\mathbf{k}'}^{\bar{a}a}(i\omega_m) \epsilon_{\mathbf{k}'-\frac{\mathbf{q}}{2}-\mathbf{Q}} \right. \\
& + \left. \frac{1}{N} \sum_{\mathbf{k}} G_{\mathbf{k}}^{\bar{a}a}(i\omega_m) \epsilon_{\mathbf{k}+\frac{\mathbf{q}}{2}-\mathbf{Q}} \frac{1}{N} \sum_{\mathbf{k}'} G_{\mathbf{k}'}^{\bar{a}a}(i\omega_m) \epsilon_{\mathbf{k}'+\frac{\mathbf{q}}{2}-\mathbf{Q}} \right\} \\
& - \frac{\pi T}{2} \sum_m \sum_a [\Sigma_m^a - U n_f^a + U(n_f^a - n_{\bar{f}}^a)] \frac{1}{N} \sum_{\mathbf{k}} G_{\mathbf{k}}^{aa}(i\omega_m) (\epsilon_{\mathbf{k}-\frac{\mathbf{q}}{2}-\mathbf{Q}}^2 + \epsilon_{\mathbf{k}+\frac{\mathbf{q}}{2}-\mathbf{Q}}^2).
\end{aligned} \tag{A.6}$$

The summations over momentum can be explicitly performed as follows:

$$\begin{aligned}
\frac{1}{N} \sum_{\mathbf{k}} G_{\mathbf{k}}^{\bar{a}a}(i\omega_m) \epsilon_{\mathbf{k}-\frac{\mathbf{q}}{2}-\mathbf{Q}} &= X' [\bar{Z}_m F_{\infty}(\bar{Z}_m) - 1]; \\
\frac{1}{N} \sum_{\mathbf{k}} G_{\mathbf{k}}^{aa}(i\omega_m) \epsilon_{\mathbf{k}-\frac{\mathbf{q}}{2}-\mathbf{Q}}^2 &= \frac{Z_m^{\bar{a}}}{Z_m} \left\{ \frac{t^{*2}}{2} (1 - X'^2) F_{\infty}(\bar{Z}_m) + X'^2 \bar{Z}_m [\bar{Z}_m F_{\infty}(\bar{Z}_m) - 1] \right\}; \\
\frac{1}{N} \sum_{\mathbf{k}} G_{\mathbf{k}}^{\bar{a}a}(i\omega_m) \epsilon_{\mathbf{k}-\frac{\mathbf{q}}{2}-\mathbf{Q}}^2 (\epsilon_{\mathbf{k}-\mathbf{q}} - \epsilon_{\mathbf{k}}) &= \frac{t^{*2}}{2} (1 - X) [\bar{Z}_m F_{\infty}(\bar{Z}_m) - 1] \\
&- X'^2 (1 - X) \left[\frac{3}{2} t^{*2} [\bar{Z}_m F_{\infty}(\bar{Z}_m) - 1] - \bar{Z}_m^2 [\bar{Z}_m F_{\infty}(\bar{Z}_m) - 1] + \frac{t^{*2}}{2} \right];
\end{aligned} \tag{A.7}$$

where

$$Z_m^a = i\omega_m + \mu_d^a - \Sigma_m^a. \tag{A.8}$$

Finally, the sum rule (first moment of the response function) contains two contributions

$$I = I_K + I_{\Pi}. \tag{A.9}$$

The first contribution comes from the kinetic energy term

$$\begin{aligned}
I_K = & 2(1 - X) \int_{-\infty}^{+\infty} d\omega f(\omega) \text{Im} \left\{ \frac{t^{*2}}{2} [\bar{Z}(\omega) F_{\infty}[\bar{Z}(\omega)] - 1] \right. \\
& \left. - X'^2 \left[\frac{3}{2} t^{*2} [\bar{Z}(\omega) F_{\infty}[\bar{Z}(\omega)] - 1] - \bar{Z}^2(\omega) [\bar{Z}(\omega) F_{\infty}[\bar{Z}(\omega)] - 1] + \frac{t^{*2}}{2} \right] \right\}
\end{aligned} \tag{A.10}$$

and the second one comes from the potential-energy term

$$\begin{aligned}
I_{\Pi} = & \int_{-\infty}^{+\infty} d\omega f(\omega) \text{Im} \sum_a \left\{ [\Sigma^a(\omega) - U n_f^a] \left(\frac{t^{*2}}{2} (1 - X'^2) G^a(\omega) + X'^2 Z^{\bar{a}}(\omega) [\bar{Z}(\omega) F_{\infty}[\bar{Z}(\omega)] - 1] \right. \right. \\
& \left. \left. - X'^2 \frac{[\bar{Z}(\omega) F_{\infty}[\bar{Z}(\omega)] - 1]^2}{G^a(\omega)} \right) + U(n_f^a - n_{\bar{f}}^a) \left(\frac{t^{*2}}{2} (1 - X'^2) G^{aa}(\omega) + X'^2 Z^{\bar{a}}(\omega) [\bar{Z}(\omega) F_{\infty}[\bar{Z}(\omega)] - 1] \right) \right\}.
\end{aligned} \tag{A.11}$$

Using the identities $\bar{Z}(\omega) F_{\infty}[\bar{Z}(\omega)] - 1 = \lambda^A(\omega) G^{AA}(\omega) = \lambda^B(\omega) G^{BB}(\omega)$ and $[G^{aa}(\omega)]^{-1} = Z^a(\omega) - \lambda^a(\omega)$, we can rewrite the potential-energy

term contribution in the final form of Eq. (68), where we use the fact that in equilibrium $\mu_d^A = \mu_d^B$ and $Z^A(\omega) - Z^B(\omega) = \Sigma^B(\omega) - \Sigma^A(\omega)$.

¹ S. Tajima, S. Uchida, A. Masaki, H. Takagi, K. Kitazawa, S. Tanaka, and A. Katsui, Phys. Rev. B **32**, 6302 (1985);

S. Tajima, S. Uchida, A. Masaki, H. Takagi, K. Kitazawa,

- S. Tanaka, and S. Sugai, *Phys. Rev. B* **35**, 696 (1987); S. Sato, S. Tajima, H. Takagi, and S. Uchida, *Nature* **338**, 241 (1989); S.H. Blanton, R.T. Collins, K.H. Kelleher, L.D. Rotter, Z. Schlesinger, D.G. Hinks, and Y. Zheng, *Phys. Rev. B* **47**, 996 (1993); M.A. Karlow, S.L. Cooper, A.L. Kotz, M.V. Klein, P.D. Han, and D.A. Payne, *Phys. Rev. B* **48**, 6499 (1993); R.P.S.M. Lobo and F. Gervais, *Phys. Rev. B* **52**, 13294 (1995); Hyun-Tak Kim, *Phys. Rev. B* **54**, 90 (1996); S.M. Hasanuzzaman, Kaoru Iwano, and Keiichiro Nasu, *J. Phys. Soc. Japan* **68**, 1376 (1999).
- ² S. R. Hassan and H. R. Krishnamurthy, *Phys. Rev. B* **76**, 205109 (2007).
 - ³ O. P. Matveev, A. M. Shvaika, and J. K. Freericks, *Phys. Rev. B* **77**, 035102 (2008).
 - ⁴ L. M. Falicov and J. C. Kimball, *Phys. Rev. Lett.* **22**, 997 (1969).
 - ⁵ U. Brandt and C. Mielsch, *Z. Phys. B: Condens. Matter* **75**, 365 (1989).
 - ⁶ J. K. Freericks and V. Zlatić, *Rev. Mod. Phys.* **75**, 1333 (2003).
 - ⁷ U. Brandt and C. Mielsch, *Z. Phys. B: Condens. Matter* **79**, 295 (1990).
 - ⁸ W. Metzner and D. Vollhardt, *Phys. Rev. Lett.* **62**, 324 (1989).
 - ⁹ P. G. J. van Dongen, *Phys. Rev. B* **45**, 2267 (1992).
 - ¹⁰ L. Chen, B. A. Jones, and J. K. Freericks, *Phys. Rev. B* **68**, 153102 (2003).
 - ¹¹ C. Gruber, N. Macris, P. Royer, and J. K. Freericks, *Phys. Rev. B* **63**, 165111 (2001).
 - ¹² B. S. Shastry and B. I. Shraiman, *Phys. Rev. Lett.* **65**, 1068 (1990); *Int. J. Mod. Phys. B* **5**, 365 (1991).
 - ¹³ J. K. Freericks and T. P. Devereaux, *Condens. Matter. Phys.* **4**, 149 (2001); *Phys. Rev. B* **64**, 125110 (2001).
 - ¹⁴ A. M. Shvaika, O. Vorobyov, J. K. Freericks, and T. P. Devereaux, *Phys. Rev. B* **71**, 045120 (2005).
 - ¹⁵ A. Khurana, *Phys. Rev. Lett.* **64**, 1990 (1990).
 - ¹⁶ A. M. Shvaika, *Physica C* **341–348**, 177 (2000); J. K. Freericks and P. Miller, *Phys. Rev. B* **62**, 10022 (2000); A. M. Shvaika, *J. Phys. Studies* **5**, 349 (2001).
 - ¹⁷ V. Janiš, *J. Phys.: Condens. Matter* **15**, L311 (2003).
 - ¹⁸ T. P. Devereaux, G. E. D. McCormack, and J. K. Freericks, *Phys. Rev. B* **68**, 075105 (2003).
 - ¹⁹ J. K. Freericks, T. P. Devereaux, M. Moraghebi, and S. L. Cooper, *Phys. Rev. Lett.* **94**, 216401 (2005).
 - ²⁰ J.K. Freericks and T.P. Devereaux, *Physica B* **378–380**, 650 (2006).
 - ²¹ C. S. Snow, J. F. Karpus, S. L. Cooper, T. E. Kidd, and T.-C. Chiang, *Phys. Rev. Lett.* **91**, 136402 (2003); H. Barath, M. Kim, J. F. Karpus, S. L. Cooper, P. Abbamonte, E. Fradkin, E. Morosan, and R. J. Cava, *Phys. Rev. Lett.* **100**, 106402 (2008).